

# Dalton Transactions

An international journal of inorganic chemistry

Accepted Manuscript

This article can be cited before page numbers have been issued, to do this please use: C. Bisio, J. Brendle, S. Cahen, Y. Feng, S. Hwang, M. Nocchetti, D. O'Hare, P. Rabu, K. Melanova and F. Leroux, *Dalton Trans.*, 2024, DOI: 10.1039/D4DT00757C.



This is an Accepted Manuscript, which has been through the Royal Society of Chemistry peer review process and has been accepted for publication.

Accepted Manuscripts are published online shortly after acceptance, before technical editing, formatting and proof reading. Using this free service, authors can make their results available to the community, in citable form, before we publish the edited article. We will replace this Accepted Manuscript with the edited and formatted Advance Article as soon as it is available.

You can find more information about Accepted Manuscripts in the [Information for Authors](#).

Please note that technical editing may introduce minor changes to the text and/or graphics, which may alter content. The journal's standard [Terms & Conditions](#) and the [Ethical guidelines](#) still apply. In no event shall the Royal Society of Chemistry be held responsible for any errors or omissions in this Accepted Manuscript or any consequences arising from the use of any information it contains.

## Data availability statement

View Article Online  
DOI: 10.1039/D4DT00757C

Manuscript Ms. Ref. No.: DT-PER-03-2024-000757 entitled "*Recent Advances and Perspectives for Intercalation Compounds Part 2: Applications in the field of catalysis, environment and health*", authored by *Chiara Bisio, Jocelyne Brendlè, Sébastien Cahen, Yongjun Feng, Seong-Ju Hwang, Morena Nocchetti, Dermot O'Hare, Pierre Rabu, Klara Melanova, Fabrice Leroux*.

No primary research results, software or code have been included and no new data were generated or analysed as part of this review.



Please do not adjust margins

View Article Online  
DOI: 10.1039/D4DT00757C

## Perspectives

## Recent Advances and Perspectives for Intercalation Layered Compounds

## Part 2: Applications in the field of catalysis, environment and health

Chiara Bisio,<sup>a,b\*</sup> Jocelyne Brendlè,<sup>c\*</sup> Sébastien Cahen,<sup>d</sup> Yongjun Feng,<sup>e</sup> Seong-Ju Hwang,<sup>f</sup> Morena Nocchetti,<sup>g\*</sup> Dermot O'Hare,<sup>h</sup> Pierre Rabu,<sup>i</sup> Klara Melanova,<sup>m</sup> Fabrice Leroux<sup>k\*</sup>

Intercalation compounds represent a unique class of materials that can be anisotropic (1D and 2D-based topology) or isotropic (3D) by their guest/ host superlattice repetitive organization. Intercalation refers to the reversible introduction of guest species with variable nature into a crystalline host lattice. Different host lattice structures have been used for the preparation of intercalation compounds and a lot of examples are given by exploiting the flexibility and the ability of 2D-based hosts to accommodate different guest species, spanning from ions to complex molecules. This reaction is then carried out to allow a systematic control and a fine tuning of the final properties of the derived compounds thus allowing to use them for various applications. This review mainly focuses on the recent applications of intercalation layered compounds (ILCs) based on layered clays, zirconium phosphates, layered double hydroxides and graphene as heterogeneous catalysts, for environmental purposes and health, aiming at collecting and discussing how intercalation processes can be exploited for the selected applications.

The intercalation is a way to specifically tune the structure, composition, and physico-chemical properties of materials by exploiting interactions between a host matrix (generally a 2D-layered material) and guest species of various chemical nature. Intercalation materials then represent a broad class of compounds generated by the reversible insertion of guest species, which can range from ions to organic species, into a layered host matrix that can have either an amorphous or crystalline structure. As a result of the intercalation procedure, the structure of the host remains normally unmodified, or it is only slightly modified in the guest-host complex. The intercalation reaction can be chemically or thermally reversible and it can be carried out using different approaches including insertion, introduction or topotactic exchange of atomic or molecular species inside the host matrix, thus allowing a controlled and systematic tuning of their physico-chemical properties.

As a general feature, intercalation layered compounds (ILCs) prepared by the different methods described in the first part of this perspective work, are a class of very flexible compounds because the appropriate choice of host and guest species results in the possibility to tune their final properties, thus spreading their potential application to numerous technological fields.

These materials can be suitable for many applications, for instance as catalysts, sorbents, electrochromic displays, electrodes for secondary batteries (Li-ion batteries), components for fuel cells and drug delivery systems. The different intercalation approaches can be indeed used to: i) modify the catalytic, optic, electronic and magnetic performances of different host structures though the introduction of

<sup>a</sup>Dipartimento di Scienze e Innovazione Tecnologica, Università del Piemonte Orientale, Viale Teresa Michel 11, 15121 Alessandria (AL), Italy; [chiara.bisio@uniupo.it](mailto:chiara.bisio@uniupo.it)

<sup>b</sup>CNR-SCITEC Istituto di Scienze e Tecnologie Chimiche "Giulio Natta", Via C. Golgi 19, 20133 Milano (MI), Italy.

<sup>c</sup>Institut de Science des Matériaux de Mulhouse CNRS UMR 7361, Université de Haute-Alsace, Université de Strasbourg, 3b rue Alfred Werner, 68093 Mulhouse CEDEX, France; [Jocelyne.brendle@uha.fr](mailto:Jocelyne.brendle@uha.fr)

<sup>d</sup>Institut Jean Lamour, UMR 7198 CNRS – Université de Lorraine, Faculté des Sciences et Technologies, B.P. 70239, 54506 Vandœuvre-lès-Nancy cedex, France.

<sup>e</sup>State Key Laboratory of Chemical Resource Engineering, Beijing Engineering Center for Hierarchical Catalysts, University of Chemical Technology, No. 15 Beisanhuan East Road, Beijing, 100029 China.

<sup>f</sup>Department of Materials Science and Engineering, College of Engineering, Yonsei University, Seoul 03722, Republic of Korea.

<sup>g</sup>Department of Pharmaceutical Sciences, University of Perugia, Via del Liceo 1, 06123 Perugia, Italy; [morena.nocchetti@unipg.it](mailto:morena.nocchetti@unipg.it)

<sup>h</sup>Chemistry Research Laboratory, University of Oxford Department of Chemistry, 12 Mansfield Road, Oxford, OX1 3TA, United Kingdom.

<sup>i</sup>Institut de Physique et Chimie des Matériaux de Strasbourg, CNRS – Université de Strasbourg, UMR7504, 23 rue du Loess, BP43, 67034 Strasbourg cedex 2, France

<sup>j</sup>Joint Laboratory of Solid State Chemistry, Faculty of Chemical Technology, University of Pardubice, Studentská 84, 53210 Pardubice, Czech Republic, [klara.melanova@upce.cz](mailto:klara.melanova@upce.cz)

<sup>k</sup>Institut de Chimie de Clermont-Ferrand, Université Clermont Auvergne, UMR CNRS 6296, Clermont Auvergne INP, 24 av Blaise Pascal, BP 80026, 63171 Aubière cedex, France; [fabrice.leroux@uca.fr](mailto:fabrice.leroux@uca.fr)

\*Corresponding authors

## Introduction

Please do not adjust margins



Please do not adjust margins

specific functionalities; ii) thermally stabilise and protect the guest species from light and oxygen; iii) develop multifunctional carriers for specific applications.

In this review, representative examples from the state of the art of the last 8 years (since 2015) on the applications of intercalation materials in the field of catalysis, environment, health and polymeric composites is reported.

This perspective is especially focused on selected cationic and anionic layered materials as host matrices for the preparation of intercalation compounds.

Emphasis is deserved on the use cationic layered materials such as clays, from both natural and synthetic origin (Fig. 1) and zirconium phosphates (ZrP). Layered double hydroxides (LDHs) are considered for the class of anionic layered materials (Fig. 2). Some recent examples on ILCs derived from graphene are also reported.

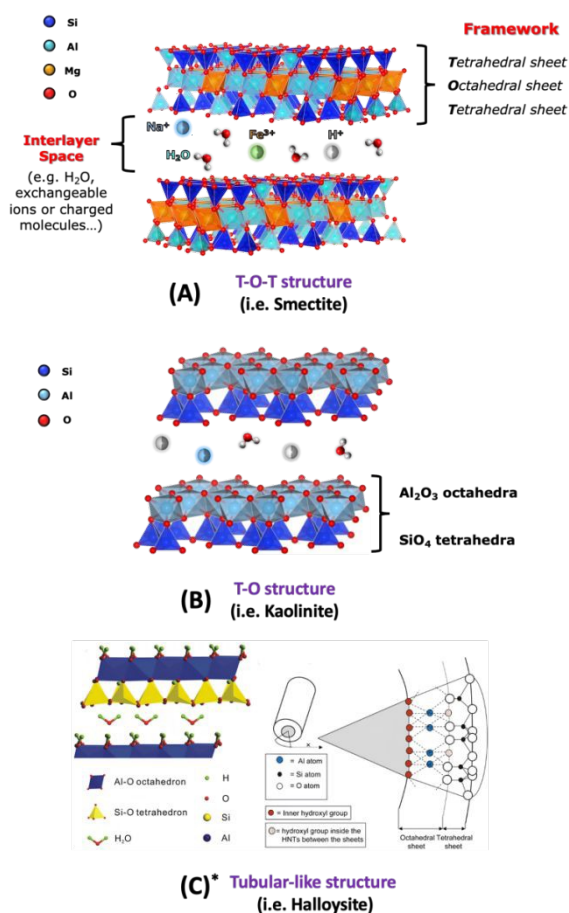


**Fig. 1** Schematic view of different clay structures: T-O-T (A), T-O (B) structures and tubular-like structure (C\* is adapted with permission from Ref. 1., Copyright 2020 MDPI).

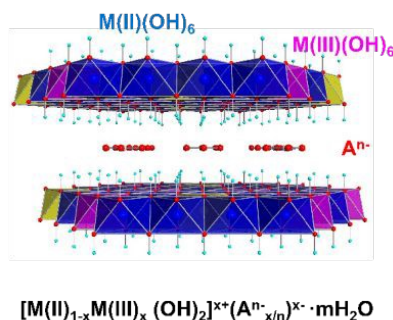
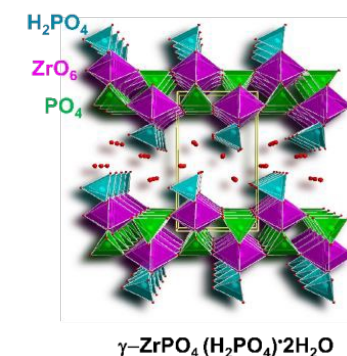
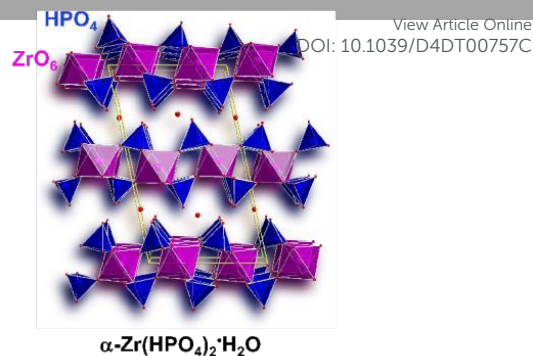


**Fig. 2** Schematic view of  $\alpha$ -ZrP,  $\gamma$ -ZrP and LDHs structures.

In the last decade, the number of scientific manuscripts of solids based on clays, ZrP, LDH for the applications of interest (e.g. heterogeneous catalysis, environment and health) deserved high attention. The amount of papers dealing with the use of selected matrices for the different applications is reported in the histograms of Fig. 3.



Please do not adjust margins

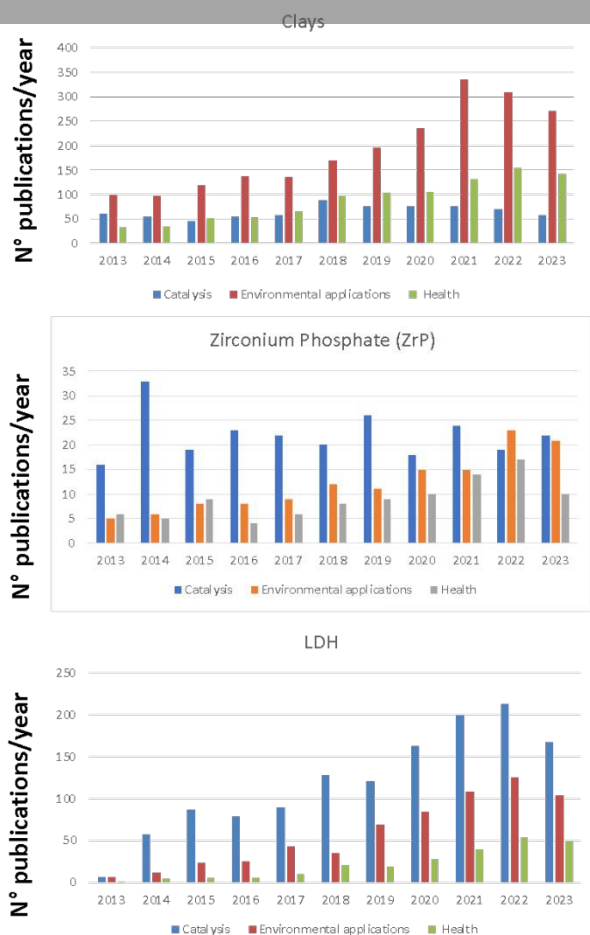


**Fig. 3** Histograms reporting the amount of publications/year for clays, LDHs and ZrP for the selected applications. Data are obtained from SCOPUS database.

In following sections, the contributions of the selected solids on the different applications are reported, focusing the attention to ILCs prepared by using clays, ZrP, LDHs and graphene.

### 1. Catalytic applications of intercalation compounds

In this section particular emphasis will be given to the description of recent applications of intercalation compounds based on clays, ZrP and LDHs for heterogeneous catalysis.

#### 1.1 Clay-based catalysts

Modified cationic clays (*e.g.* acid treated clays) have been used in oil cracking reactions from 1930s. Their use for catalytic purposes was then partially substituted with zeolites and porous materials from 1960s. However, modification process such as acid activation, ion exchange, pillaring procedures, preparation of composites and hybrids or hierarchically structuration of clays allowed the preparation of different families of intercalation compounds proposed as heterogeneous catalysts.<sup>1,2</sup>

Clay-based catalysts have been used in the conversion of crude oil to biodiesel and they are employed as catalysts for several reactions

such as esterification, addition, transesterification, oxidation, hydrogenation, epoxidation, alkylation, polymerisation, allylation, diazotisation, acylation, rearrangement, isomerisation, cyclisation condensation, organic synthesis etc.<sup>3,4</sup> It was pointed out that catalysts derived from layered silicate are regenerable, low-cost and active not only to produce biodiesel but also for other chemical processes such as oxidation reactions, water treatment and photovoltaic applications. These solids showed efficient catalytic potential, allowing a high yield of FAMES (Fatty Acid Methyl Esters) at less harsh reaction conditions, they are proved to be easily recoverable, highly reusable and thus highly sustainable.<sup>2</sup>

Among clays, halloysite-based (HNTs) heterogeneous catalysts deserve additional comments. Composite and hybrid materials obtained by a surface modification of halloysite, a natural clay with tubular morphology, are largely proposed in the literature. It was observed that the synergy between halloysite and different modifying species (*i.e.* polymers, dendrimers, porphyrin, MOFs., ionic liquids) allow to increase the performances of the final hybrid/composite. However, the use of halloysite-based hybrids/composites is also related to some disadvantages due to the time-consuming multistep production processes, often involving (toxic) solvents/reagents for the large-scale production of these materials.<sup>5</sup> Modified halloysite have been also proposed for environmental and catalytic applications. For this latter application, the presence of metal nanoparticles (NPs) is essential to impart catalytic performances. Besides methods allowing to introduce NPs on the outer surface of halloysite, the methods to embed metallic NPs of small size in the inner part of HNTs have been recently reviewed.<sup>6</sup> These methods have the advantage to increase the resistance of NPs to cleavage and agglomeration of the embedded metallic NPs, thus improving the catalytic activity of the obtained solid.

Jiang et al. prepared Pd/HNTs exploiting a modification of hydrophobicity of halloysite by impregnating the solid with CTAB species (see Fig. 4). The proposed method allowed to obtain uniformly dispersed palladium particles (*ca.* 2 nm), with a suitable ratio of Pd<sup>2+</sup>/Pd<sup>4+</sup> species and appropriate surface acidity: this solid showed improved catalytic activity with respect to catalyst prepared without adding CTAB.<sup>7</sup>

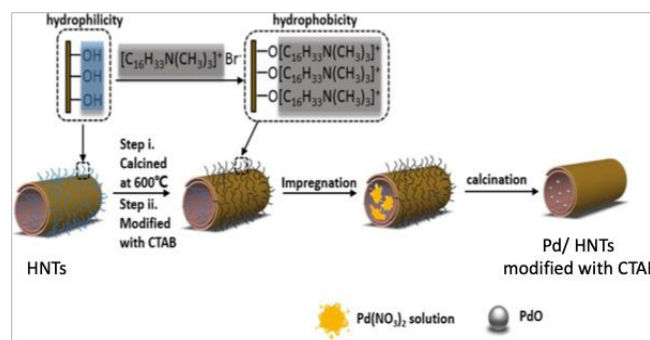


**Fig. 4** Schematic diagram of the preparation method of Pd/HNTs catalyst. Adapted with permission from Ref. 7. Copyright 2020, American Chemical Society.



Please do not adjust margins

For methane combustion, high-performance halloysite-supported palladium catalysts have been also proposed through proper pre-treatments of the support.<sup>8</sup>

Cu-Ni containing halloysite solids prepared by ligand-assisted reduction of Cu<sup>2+</sup> and Ni<sup>2+</sup> cations followed by annealing have been also tested the purification of vehicle exhaust gases through catalysed processes.<sup>9</sup> For this process, catalysts based on confinement of Cu-Ni species, Pd, Ag (particle size below 3 nm) have been proposed. It was shown that the nano-confinement allows to increase the stability of embedded NPs to detachment and sintering, also improving the catalytic reaction kinetics.<sup>6</sup>

The modification of clays chemical composition was also proposed to introduce catalytic active sites in the clay framework thus leading to active materials for the catalytic decomposition and/or simultaneous detection of toxic molecules, *i.e.* chemical warfare agents.<sup>10-12</sup> In these cases, the synergistic presence of proton sites (normally introduced by ion exchange in acidic aqueous solutions) and metal centres (either present naturally in clays or introduced by modifying the preparation steps of the support) are beneficial for the catalytic performances of the final material.

Thermally stable pillared clays (or Pillared Interlayered Clays, PILCs) derive from the intercalation of inorganic polycations in the clay interlayer space. The clay pillaring procedure allowed the preparation of solids mainly based on transition metal species with large interest in the catalytic purposes especially required in advanced oxidation processes and chemical transformations. Pillaring procedure allows to introduce specific catalytic species on clays surface and this, together with the improvement of specific surface area and thermal stability, makes these solids suitable for different catalytic reactions (*e.g.* nitration of chlorobenzene, catalytic combustion of acetone, methyl-ethyl-ketone) oxidation and isomerization reactions and as Fenton-like systems for the degradation of organic pollutants in wastewaters.<sup>13</sup> Clays pillared with TiO<sub>2</sub> (Ti-PILC) are characterised by surface acidity higher than other pillared clays, such as Al or Zn-PILC.<sup>13</sup> The origin of Brønsted and Lewis acid sites in Ti-PILC have been largely studied.<sup>14</sup> Photocatalytic degradation of organic species (*i.e.* organic dyes, herbicides and aromatic amines, phenolic compounds, emerging contaminants) over PILCs with TiO<sub>2</sub> species has been recently reviewed giving particular emphasis on photocatalysts based on kaolinite, palygorskite, montmorillonite and halloysite.<sup>15</sup>

Very recently, the use of PILC for the catalytic reduction of NO<sub>x</sub> with hydrocarbons at low temperature was reviewed.<sup>16</sup> Special interest was given to metal-supported PILC and the catalytic performances of different samples together with the possible reaction mechanisms in relation to the different active sites, metal loading and reaction conditions is reported. It was underlined that Ag- and Cu-based PILC displayed good performances for NO<sub>x</sub> conversion in the presence of short hydrocarbons (HC) at low temperature. Nevertheless, additional studies are needed to better clarify the HC-SCR reaction mechanisms in the presence of metal-modified PILC catalysts. Major challenges are represented by the preparation of stable metal-

modified PILC catalysts for NO<sub>x</sub> reduction in the presence of H<sub>2</sub>O and SO<sub>2</sub>.<sup>16</sup>

View Article Online  
DOI: 10.1039/D4DT00757C

Moreover, TiO<sub>2</sub>/clays heterostructures for the remediation of water polluted from organic species have been recently proposed.<sup>17</sup> In this respect, particular emphasis was done to the use of phyllosilicates as supports (*e.g.* montmorillonite, sepiolite, palygorskite, vermiculite, saponite). The introduction of pillars in the clays galleries results in a stable porosity leading to heterostructured materials with high specific surface area (SSA) characterised by the presence of micro- and mesopores. The pore architecture and the high SSA have a positive effect on the photocatalytic activity of TiO<sub>2</sub>/clay materials. Moreover, long-chain hydrophobic cationic surfactants can be exploited to tune the porosity of TiO<sub>2</sub>-based clays and to produce Porous Clay Heterostructures (PCHs) and Delaminated Porous Clay Heterostructures (DCPHs).<sup>18-20</sup>

These composite materials have been proposed to overcome the problems related to the practical and environmental issues linked to the use of nanosized TiO<sub>2</sub> powders. Different clays such as kaolinite, hectorite, saponite, montmorillonite, palygorskite, halloysite and imogolite have been proposed as support materials for TiO<sub>2</sub> nanoparticles, thus obtaining solids with high photocatalytic efficiency and easy separation from treated water. The different examples reported in the literature suggested that the combination of clay support, characterised by high specific surface areas and adsorption capacity improves the photocatalytic activity of TiO<sub>2</sub> nanoparticles and thus the decomposition capacity of organic pollutants. It was pointed out that the anchoring of TiO<sub>2</sub> on clays surface is useful to reduce the TiO<sub>2</sub> agglomeration, thus leading to more active surface sites.<sup>15</sup>

A schematic representation of the formation of PILC and PCH starting from intercalation processes is reported in Fig. 5.

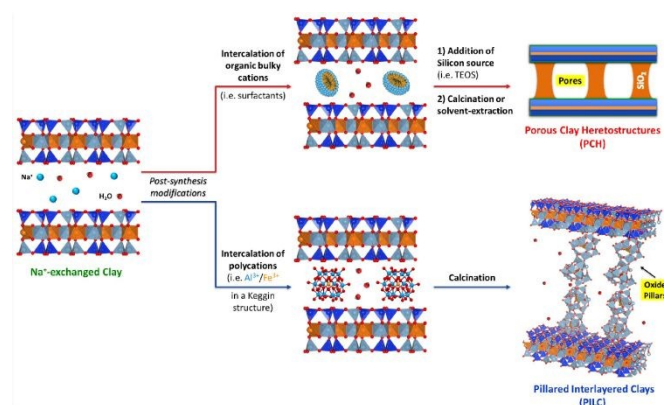


**Fig. 5** Schematic view of the intercalation processes leading to the formation of Porous Clay Heterostructures (PCH) and Pillared Interlayered Clays (PILC).



Please do not adjust margins

### 1.2 Catalytic applications of zirconium phosphate (ZrP)

ZrP can be also considered as promising materials for catalytic applications. ZrP shows very interesting physical and chemical properties, such as high ion-exchange capacity, good chemical and thermal stability, and easy functionalization. The presence of acidic P-OH groups on the layers makes this solid an efficient catalyst in acid-catalyzed reactions. The acidity and the hydrophobicity of ZrP surface can be modulated by totally or partially replacing the phosphate groups with other phosphonate groups. The modification of the ZrP surface has also been achieved by exploiting the reactivity of the surface hydroxyl groups with organofunctional silanes that allowed to immobilise catalytically active nanoparticles.<sup>21,22</sup> Moreover, several catalysts have been prepared considering the ion-exchange capacity of ZrP. Intercalation compounds containing metal ions or metal complexes have shown good performance as catalysts for converting biomass-derived molecules in added-value products as oxygenated fuels and fine chemicals. In particular, ZrP-Ru(III) and Ni/ZrP (Fig. 6A) showed high catalytic activity towards the oxidation of 5-hydroxymethylfurfural (HMF) under mild conditions.<sup>23,24</sup> ZrP intercalated with Ru(II) complex ( $[(p\text{-cymene})\text{Ru}(\text{phen})\text{Cl}]\text{Cl}$ ) showed higher catalytic performance in selective hydrogenation, with molecular  $\text{H}_2$ , of the C=O group of furfural and of other carbonyl compounds into the corresponding alcohols. Experimental study and DFT calculation gave evidence that the catalytic performance can be attributed to the interaction of -POH groups of ZrP and Ru complex, leading to Ru-O-P active species.<sup>25</sup> Cu/ZrP catalyst enabled the direct oxidation of phenol, also derived from lignin depolymerization, to *cis,cis*-muconic acid that can be converted further into high-added value chemicals.<sup>26</sup>

Composites ZrP/silver-based materials are obtained by exploiting the intercalation properties of ZrP and then used as catalysts for organic pollutants degradation. Silver exchanged ZrP treated with halogenidric acids gave rise to ZrP/AgX (X=Cl and Br) composites able to catalyze photodegradation of Rhodamine B (RhB). The action of ZrP as a source of silver ions led to a reduction of AgCl particle growth and aggregation, thus increasing the number of catalytic active sites. In addition, the -POH groups of ZrP promote the chemisorption of the RhB and then its degradation.<sup>27,28</sup> A composite ZrP-polydopamine (ZrP@PDA) was prepared by polymerization of dopamine in the aqueous dispersion of exfoliated ZrP. The catechol groups of PDA reduced the noble metal ions, such as silver or gold, generating metallic NPs on the ZrP@PDA surface. These composites showed very interesting catalytic activity towards the reduction of 4-nitrophenol to 4-aminophenol (Fig. 6 B).<sup>29,30</sup> The exfoliation/restacking method was exploited to immobilise Pd precursor ( $\text{Pd}(\text{NH}_3)_4\text{Cl}_2$ ) on  $\alpha$ -ZrP nanosheets. The treatment with a reducing agent gave rise to Pd NPs, with an average diameter of 5.17 nm, immobilised on ZrP nanosheets (Fig. 6 C). The composite showed good performance as heterogeneous catalyst for the Heck reaction.<sup>31</sup> Due to the ZrP electrochemical inertness it has been studied as a support for transition metals for the electrocatalysis of oxygen evolution reaction (OER) in alkaline media.<sup>32</sup> Ions  $\text{Fe}^{2+}$ ,  $\text{Fe}^{3+}$ ,  $\text{Co}^{2+}$ , and  $\text{Ni}^{2+}$  were intercalated or adsorbed on  $\alpha$ -ZrP material. The systems

display an interesting activity for the OER, requiring between 0.5–0.7 V of overpotential to reach  $10 \text{ mA/cm}^2$  (benchmark for OER catalyst activity). It was found that the OER occurs especially on the external surfaces of the nanoparticles thus the catalytic activity increases upon the exfoliation of ZrP materials.<sup>33</sup> Moreover, the OER activity depends on the loading and coverage of cobalt and nickel on the ZrP with different morphology.<sup>34</sup> More recently, mixtures of nickel–iron were confined in ZrP; the hydrated confined environment of the layered structure stabilise Fe-rich compositions yielding highly active OER catalysts.<sup>35</sup> Carbon-free electrocatalysts for oxygen reduction reaction in polymer electrolyte membrane fuel cells were prepared by growing Pt nanoparticles on ZrP which is a solid-state proton conductor (Fig. 6 D). The Pt/ZrP composites showed high durability and superior performance with respect to platinum-supported carbon catalysts commercially available.<sup>36</sup>

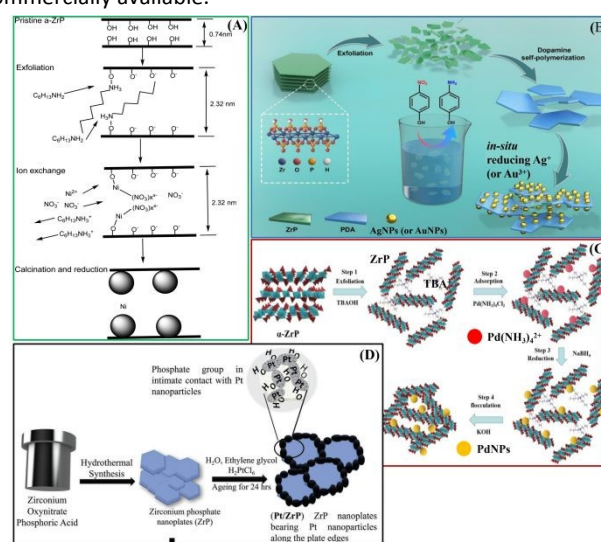


**Fig. 6** Schematic illustration of preparation steps of the catalysts: (A) Ni/ZrP adapted with permission from ref. 24, Copyright 2018 American Chemical Society; (B) ZrP@PDA/AuNP or ZrP@PDA/AuNP, adapted with permission from ref. 30, Copyright 2020 MDPI; (C) ZrP-PdNPs, Adapted with permission from ref. 31, Copyright 2022 Taiwan Institute of Chemical Engineers; (D) Pt/ZrP. Adapted with permission of ref. 36. Adapted with permission from ref. 36, Copyright 2023 John Wiley and sons.

### 1.3 Catalytic applications of LDHs

A recent review underlines the versatility of LDHs as anion-exchange framework as well as considering their ability to face today's societal issues such as their high biocompatibility combined with their relatively low impact in terms of biodegradation.<sup>37</sup> LDH are used as photocatalysis, electrocatalysis,  $\text{CO}_2$  handling, biomass conversion, lowering the anthropogenic effects on the environment as scavenger for pollutants for water and soil treatments, additives for polymer and for polymer coatings.

The importance of the use of catalysts with reduced size (nanocatalysts) is covered in an interesting review focused on the biomass conversion including reduction, oxidation or reforming reaction.<sup>38</sup> The tunability in the chemical composition of LDH associated to the



Please do not adjust margins

View Article Online

DOI: 10.1039/D4DT00757C

large choice to accommodate interleaved guests as well as their developed surface to expose and well-disperse active species (for example metals or nanoparticles in an atomic-level uniform distribution) make of LDHs-based suitable and efficient nanocatalysts.

This is exemplified with for de(hydrogenative) transformations and catalytic hydrogenations using transition metal into LDHs<sup>39</sup> and more specifically Ni-based LDH to catalytically convert bio-ethanol to butanol.<sup>40</sup> In the latter case, the aldol-condensation to use biomass and produce butanol was optimised from a supported Cu/NiAlOx material in a time-on-stream of 110 h at 280°C reaching appropriate performance in terms of ethanol conversion and butanol selectivity and catalyst stability. Adapted cation composition as well as particle size can stabilise LDHs even in acidic medium. For instance, LiAl<sub>2</sub> LDH-based sheets prepared by urea method was covered by NHC-heterocyclic carbene gold anionic complexes for a reaction of hydration of alkynes.<sup>41</sup> Another study reports LDH of Mg<sub>4</sub>Al composition covered this time by silver NP for the alkylation of nitriles, oxindoles and other carboxylic acid derivatives with alcohols.<sup>42</sup> In this study NP and LDH support are co-acting in the cyclization of N[2-(hydroxymethyl)phenyl]-2-phenylacetamides to yield 3-arylquinolin-2(1H): NP in the dehydrogenation and hydrogenation steps, while LDH support catalyses the condensation step.

LDHs are also studied as photocatalyst, a recent review covers the latest advances in that domain<sup>43</sup> as well as electrocatalysts, mostly for the water splitting to produce green hydrogen as other compounds family such as transition metal chalcogenides.<sup>44</sup> As far as water electrolysis are concerned, they should possess electrocatalytic activity associated to a long-term stability. LDHs rank well for developing such sustainable and clean energy as discussed in critical reviews,<sup>45,46</sup> where the relationship between structural defects and electrocatalytical performances are scrutinised, as for Ce-doped NiFe LDHs-based material disposed onto carbon paper<sup>47</sup> or NiFe heterostructure nanorods<sup>48</sup> for the OER. Other interesting articles mainly focus on LDHs as well as the possibility for seawater electrolysis since they are stable in alkaline electrolyte suitable for the seawater oxidation at the anode through the OER and not that of chloride ions.<sup>49</sup> However, NiFe LDHs-based electrocatalysts for OER suffer from instability upon cycling mostly due to the leaching of Fe active sites migrating out of the structure to form ferrihydrite by-product after repetitive potential cycling.<sup>50</sup>

Among 2D carbon-based materials, iron- and nitrogen-doped graphene appears as promising platinum-free materials for oxygen reduction reaction (ORR),<sup>51</sup> g-C<sub>3</sub>N<sub>4</sub> and other doped graphenic materials (i.e. single or double doping with N, B, S and P) for ORR, hydrogen evolution (HER), and OER rivalling that of noble metals and transition metal-based catalysts have been reviewed by Chen *et al.*<sup>52</sup>

The examples described above are summarised in Table 1. Wherever possible, the comparison of catalytic performances of ILCs are compared with those of reference materials (*e.g.* non-hybridised systems, non-intercalated heterogeneous catalysts).





Please do not adjust margins

## Perspectives

**Table 1.** Most representative examples of intercalation compounds based on clays, ZrP and LDHs for the catalytic applications. Results described in the Reviews are not reported.

| Catalyst   | Active specie   | Catalyst preparation  | Reaction            | Substrate  | Catalytic conditions  | Products   | Ref |
|--|---|---|---------------------|--|---|--|-----|
| Pd/HTNs  | Pd  | CTAB surface modification, impregnation and calcination                                 | oxidation           | methane  | 0.2 g catalysts with 1wt% Pd nominal loading;<br>Gas feed: 1 vol % CH <sub>4</sub> , 10 vol % O <sub>2</sub> in N <sub>2</sub><br>Flow rate: 100 mL/min<br>T: 425-620°C | Methane conversion: 99% at 425 °C, ca. 195 °C lower than of Pd/HNTs prepared without any surface modification                                | 7   |
| Pd/HNTs  | Pt  | Surface modification using acid, basic media and surfactants, impregnation, calcination | oxidation           | methane  | 50 mg catalysts CH <sub>4</sub> :O <sub>2</sub> :Ar (1%:20%:79%)<br>Flow rate: 60 mL/min<br>T: 250-450°C  | Methane conversion depends on the surface treatment. Best performances with Pd/HNTs-NaOH that shows 90% conversion at 373 °C.                | 8   |
| Cu-Ni/HTNs   | Metallic Cu and Ni particles                                    | Wet chemical synthesis  | reduction           | simulated exhaust gas (equimolar mixture of nitrogen monoxide and carbon monoxide) | 10 mg catalysts, NO (5.00 kPa) and CO (5.00 kPa)<br>T: 275-400°C  | NO conversion to N <sub>2</sub> : over 90% at 325°C after 30 min.  | 9   |
| Nb/saponite<br>Synthetic saponite clay                                       | Nb in framework position<br>Intercalated H <sup>+</sup> species | Nb introduction in framework position   | Selective oxidation | 2-chloroethyl)ethylsulfide (CEES)  | 20 mg catalyst<br>14 mM CEES; 70 mm30% aq. H <sub>2</sub> O <sub>2</sub> ; <i>n</i> -heptane;<br>T: 25°C  | CEES conversion: 98% (8h)<br>Selectivity to CEESO: 73%<br><br>Synthetic saponite clay (without Nb and protons): CEES conversion ca. 20% (8h) | 10  |
| Fe/montmorillonite<br>H/ montmorillonite<br>Commercial (non modified) sample | Fe <sup>3+</sup> and H <sup>+</sup>                             | Ion exchange of montmorillonite natural clay  | Selective oxidation | 2-chloroethyl)ethylsulfide (CEES)  | 20 mg catalyst<br>14 mM CEES; 70 mm30% aq. H <sub>2</sub> O <sub>2</sub> ; <i>n</i> -heptane;<br>T: 25°C  | CEES conversion: >99% over acid sample after 48h<br><br>The parent sample (without any modification): CEES conversion of 7.5% after 48h      | 11  |

Please do not adjust margins



Please do not adjust margins

|  |   |  |                            |                          |   |  |    |
|--|---|--|----------------------------|--------------------------|---|--|----|
| TiO <sub>2</sub> -MMT PLC  | TiO <sub>2</sub>  | Intercalation of Ti alkoxide precursor with supercritical CO <sub>2</sub>                    | Photocatalytic degradation | Toluene and acetaldehyde | Toluene (100 vol ppm) and acetaldehyde (500 vol ppm) in humidified air, 250 W high-pressure mercury lamp  | VOCs decomposition rate between 2 and 6 mol/min/mol TiO <sub>2</sub>   | 18 |
| TiO <sub>2</sub> -MMT PLC<br>Compared with TiO <sub>2</sub><br>P25 | TiO <sub>2</sub>  | Acidic solutions of hydrolyzed Ti alkoxides in the presence of high-molecular-weight polymer | Photocatalytic degradation | Methylene blue (MB)      | Aqueous suspensions of MB (250 ml, initial concentration 30mg/l) and photocatalyst powder (50 mg), 250 W high-pressure mercury lamp   | Maximum removal efficiency of methylene blue is for PIL up to 83% within 90 min<br><br>For P25: degradation efficiency <i>ca.</i> 46%  | 19 |
| Multicomponent PCHs  | SiO <sub>2</sub> /Al <sub>2</sub> O <sub>3</sub> ,<br>SiO <sub>2</sub> /TiO <sub>2</sub> and<br>Si/ZrO <sub>2</sub> pillars | pillaring by surfactant directed methods and template ion exchange method.                   | Dehydration reactions      | Methanol and ethanol     | 100 mg catalysts<br>Gas mixture containing 3.9 vol% of methanol diluted in helium (total flow rate of 20 ml/min, isothermal saturator at 0 °C) or 5.7 vol% of ethanol diluted in pure helium (total flow rate of 20 ml/min, isothermal saturator at 20 °C<br>T: between 100 and 325°C | Methanol conversion to dimethyl ether (DME): between 40 and 77% at 300°C (best results obtained in the presence of SiO <sub>2</sub> pillars)<br><br>Ethanol conversion to diethyl ether (DEE) and ethylene: between 80 and 100% at 300°C (best results achieved in the presence of Al <sub>2</sub> O <sub>3</sub> pillars) | 20 |
| ZrP-Ru   | Ru(III)   | Ion-exchange   | oxidation                  | 5-hydroxymethylfurfural  | T=110 °C<br>P= atmospheric O <sub>2</sub><br>pressure, flow rate of 20 ml/min<br>t= 12 h  | 2,5-Furandicarboxylic acid (selectivity: 28%)<br>2,5-diformylfuran (selectivity: 62%)  | 23 |
| Ni/ZrP   | Ni, Lewis acidic sites of Zr(IV)  | Exfoliation, Ion-exchange, Calcination and reduction   | hydrodeoxygenation         | 5-hydroxymethylfurfural  | T=240 °C<br>P=5 MPa H <sub>2</sub><br>t= 20 h   | 2,5-dimethylfuran (yield: 68.1%)   | 24 |
| ZrP-[(p-cymene)Ru(phen)Cl]<br>Compared with: Ru/C                  | Ru-O-P species formed by interaction of cationic Ru(II)   | Exfoliation, Ion-exchange  | hydrogenation              | furfural                 | T=100°C<br>P=1.5 MPa H <sub>2</sub><br>T=8 h  | furfuryl alcohol (selectivity: 99%)<br>For Ru/C: furfuryl alcohol (selectivity: 34%)   | 25 |



Please do not adjust margins

|  | complex and P-OH group of ZrP                          |  |                              |   |  |  |    |
|--|--|--|------------------------------|---|--|--|----|
| Cu/ZrP<br>Compared with:<br>Cu(OAc) <sub>2</sub>                         | Cu(II) bound with phosphate groups, Cu(II)-O-P species | wet impregnation, calcination at 200 °C                | oxidation                    | phenol                                    | HCOOH:H <sub>2</sub> O <sub>2</sub> = 5:1, 12 mmol H <sub>2</sub> O <sub>2</sub> , 0.2 mmol H <sub>3</sub> PO <sub>4</sub><br>T= 30 °C<br>T=2 h                      | cis, cis-muconic acid (selectivity: 60%; yield: 40%)<br>For Cu(OAc) <sub>2</sub> : cis, cis-muconic acid (selectivity: 55%; yield: 35%)  | 26 |
| ZrP/AgCl<br>Compared with: AgCl  | Ag@AgCl  | Ion-exchange, treatment with HCl                       | photodegradation             | Rhodamine B                               | mg AgCl/mL RhB=0.74<br>[RhB]= 10 <sup>-5</sup> M   | chromophore cleavage: 92% in 10 min<br>For AgCl: chromophore cleavage: 57% in 30 min   | 27 |
| ZrP/AgBr<br>Compared with: AgCl  | Ag@AgBr<br>Ag@AgBr                                     | Ion-exchange, treatment with HBr                       | photodegradation             | Rhodamine B                               | mg AgBr/mL RhB=1.1<br>[RhB]= 10 <sup>-5</sup> M  | chromophore cleavage: 90% in 3 min<br>chromophore cleavage: 91% in 30 min  | 28 |
| ZrP@PDA/Ag<br>Compared with:<br>AgNPs/SNTs                               | AgNPs  | reduction and deposition of silver on ZrP-polydopamine | reduction                    | 4-nitrophenol (4NP)                       | [4NP]= 0.12 mM, [NaBH <sub>4</sub> ]= 38 mM<br>[Ag]= 0.125 µg mL <sup>-1</sup><br>T= 25 °C   | 4-aminophenol (apparent rate constant=34.76×10 <sup>-3</sup> s <sup>-1</sup> )<br>For AgNPs/SNTs: 4-aminophenol (apparent rate constant=38.41×10 <sup>-3</sup> s <sup>-1</sup> ) | 29 |
| ZrP@PDA/Au<br>Compared with:<br>Au@MOF-3                                 | AuNPs  | reduction and deposition of gold on ZrP-polydopamine   | reduction                    | 4-nitrophenol (4-NP)                      | [4NP]= 0.24 mM, [NaBH <sub>4</sub> ]= 76 mM<br>[Ag]= 0.125 µg mL <sup>-1</sup><br>T= 25 °C-  | 4-aminophenol (apparent rate constant=7.4×10 <sup>-3</sup> s <sup>-1</sup> )<br>For Au@MOF-3: 4-aminophenol (apparent rate constant=68.8×10 <sup>-3</sup> s <sup>-1</sup> )      | 30 |
| Pd@ZrP<br>Compared with: PS-TEA  | PdNPs  | Exfoliation, restacking, in-situ reduction             | Carbon-carbon bond formation | Iodobenzene (IB) and methyl acrylate (MA) | IB= 1.0 mmol<br>MA= 1.5 mmol NEt <sub>3</sub> = 1.5 mmol DMF= 2mL,<br>T= 100 °C<br>t= 0.5 h<br>Pd@ZrP= 15 mg, 0.204 mol% of Pd<br>NEt <sub>3</sub> , GVL, 130°C, 2 h | Methyl cinnamate (conversion: 95.8%)<br>For PS-TEA: Methyl cinnamate (conversion: 91%)   | 31 |
| Ni <sub>0.1</sub> Fe <sub>0.9</sub> -ZrP<br>Compared with:<br>Ni1Fe2-250 | Ni <sup>2+</sup> /Fe <sup>3+</sup>                     | Ion-exchange reaction                                  | OER                          | water                                     | Catalyst loading= 0.125 mg/cm <sup>2</sup><br>KOH= 0.1M<br>Catalyst loading = 0.17 mg/cm <sup>2</sup>  | Overpotential= 350mV at 10 mA cm <sup>-2</sup><br>For Ni1Fe2-250: Overpotential= 310mV at 10 mA cm <sup>-2</sup>   | 35 |



Please do not adjust margins

|  |   |   |  |                                    |  |  |    |
|--|---|---|--|------------------------------------|--|--|----|
| Pt/ZrP<br>Compared with: Pt/C  | PtNPs                                     | Ageing ZrP with H <sub>2</sub> PtCl <sub>6</sub>  | oxygen reduction reaction (ORR) in polymer electrolyte membrane fuel cells (PEMFC) | oxygen                             | PEMFC at an operating potential of 0.60V   | maximum power densities = 0.95 W cm <sup>-2</sup><br>For Pt/C: maximum power densities = 0.83 W cm <sup>-2</sup>   | 36 |
| Cu/NiAl-LDH  | Cu/NiAlOx                                 | hydrothermal deposition precipitation method  | Guerbet coupling reaction  | biomass-derived ethanol            | T= 280°C,<br>P= 2 MPa N <sub>2</sub><br>T= 110 h   | n-butanol (conversion= 35%, selectivity= 25%)  | 40 |
| LiAl <sub>2</sub> -LDH-NHC-Au(I)   | gold/carben complex NHC,Au (I)(NHC-Au(I)) | Direct coprecipitation  | hydration  | Alkynes alcohol (i.e. pent-4-ynol) | Catalyst= 0.75 mol%<br>T= 60°C<br>t= 2h<br>pH= 3   | 5-hydroxypentan-2-one (conversion=100%)  | 41 |
| Ag/Mg <sub>4</sub> Al-LDH  | AgNPs and LDH                             |   | Formation of new C-C bonds from alcohols and C nucleophiles                        | nitriles, oxindoles                | nitrile or oxindole = 0.125 mmol alcohol= 0.375 mmol<br>Ag/Mg <sub>4</sub> Al-LDH= 134 mg, 5 mol% Ag<br>Mesitylene= 1.5 mL<br>T= 140°C under N <sub>2</sub><br>T= 24 h     | Isolated products (yield= from 70% to 97%)   | 42 |
| NiFeCe-LDH on carbon paper (CP)<br>Compared with: commercial IrO <sub>2</sub> benchmark                  | Ni <sup>2+</sup> /Fe <sup>3+</sup>        | Precipitation with urea   | OER  | water                              | KOH= 1M<br>50 μL of the ink (IrO <sub>2</sub> = 3 mg, Nafion= 15μL, Ethanol= 1 mL)<br>was dropped on CP<br>KOH= 1 M  | Overpotential= 232mV mV at 10 mA cm <sup>-2</sup><br>For IrO <sub>2</sub> : Overpotential= 451mV at 10 mA cm <sup>-2</sup>                               | 47 |
| NiFe-LDH/Fe <sub>1</sub> -N-C heterostructure hollow nanorods<br>Compared with: Pt/C    IrO <sub>2</sub> | NiFe-LDH and Fe <sub>1</sub> -N-C         | preparation of Fe <sub>1</sub> -N-C hollow nanorods through a ZIF-phase-transition principle, decoration with NiFe-LDH nanodots | Bifunctional ORR/OER in rechargeable Zn-air batteries                              | O <sub>2</sub> /water              | catalyst (carbon cloth) as the air cathode, a zinc plate as the anode, 6 M KOH solution containing 0.2 m Zn(Ac) <sub>2</sub> filled between the electrodes as electrolyte. | power density = 205 mW cm <sup>-2</sup><br>ultralong cyclability up to 400 h<br>For Pt/C    IrO <sub>2</sub> : power density = 111.6 mW cm <sup>-2</sup> | 48 |



Please do not adjust margins

View Article Online  
DOI: 10.1039/D4DT00757C

## Perspectives

### 2. Environmental applications of intercalation materials

This section is devoted to the description of the most representative examples of intercalation compounds based on clays, ZrP and LDHs for the removal of environmental contaminants. An overview of the most significant examples of these materials for environmental applications is also reported in Table 2.

#### 2.1 Environmental applications of clays

Clays minerals have been largely studied in the last decades as solid adsorbents to remove heavy metals with high toxicity (*i.e.* cadmium, copper, lead, zinc, chromium (VI) but also mercury, cobalt, manganese, chromium (III)), organic dyes and other pollutants (*i.e.* antibiotics, PFAS, organic species...) from aqueous solutions and industrial wastewaters.<sup>53-57</sup> Natural clays are used because of their non-toxic nature, low-cost, large availability, and high adsorption capabilities. Examples of clays modification to allow the detection of specific anions are also given.<sup>58</sup>

Natural clays are very often modified by using thermal treatments, acid washing, pillaring strategies, or through the intercalation of organic species in the galleries aiming at improving adsorption properties. Materials such as clays nanosheets, nanotubes, nanorods and clay-supported nanoparticles, are reported.<sup>59</sup> In this respect, interesting recent approaches are linked to clays exfoliation processes to obtain low dimensional clays (with 1D or 2D morphology). This method is used to fully expose adsorption sites and to increase the specific surface area of the adsorbents.<sup>60,61</sup>

Moreover, coupling agents and/or polymers are used to create nano-clay based composites with a porous structure allowing to exploit the exposed adsorption sites and/or to introduce functional groups aiming at increasing the affinity to heavy metals and toxic dyes.<sup>59</sup>

Clays have been also proposed as supports for nanoparticles of metals and metal oxides (*i.e.* iron and copper oxides, TiO<sub>2</sub>, ZnO, Al<sub>2</sub>O<sub>3</sub>) thus obtaining more effective adsorbing agents. As a matter of example, the presence of Fe<sub>3</sub>O<sub>4</sub> on halloysite nanotubes have been proposed to treat the excess of phosphate in water media: it was reported that the supported metal species improves the clay surface charge density thus leading better phosphate control.<sup>62</sup> The presence of the clay seems to improve the adsorption capacity of pristine Fe<sub>2</sub>O<sub>3</sub> species towards arsenite species.<sup>63</sup>

Supported metal oxide species are also useful for the degradation of toxic species. The case of nanoparticle sized zero-valent iron (normally named nZVI or nFe<sup>0</sup>) deserved special attention in wastewater and groundwater remediation because of its ability for the degradation and removal of different metals (*i.e.* As, Cr(VI)), Pb and other toxic pollutants.<sup>64-66</sup>

The combination of nZVI and clay support is a positive strategy to avoid aggregation of metal species thus allowing the development of effective systems for water remediation. The use of these composite systems has been systematically reviewed in 2017.<sup>67</sup>

The preparation and use of several types of the clay-based composite materials towards contaminants remediation (with emphasis on heavy metals, nitrate, selenate, dyes, nitroaromatic compounds, polybrominated diphenyl ethers and chlorinated compounds) are also reported. Data related to an extended use of the type of nanocomposites for the removal of chlorinated volatile organic compounds on soils are also discussed and it was shown that concentration of pollutant species is strongly reduced.<sup>68</sup> Nevertheless, further studies to clarify the mechanism of degradation of various contaminants on nZVI/clay composites (*i.e.* adsorption, oxidation, reduction and precipitation processes) are still needed, even to optimise optimum preparation and application conditions of these materials.

Intercalation of natural clays with surfactants (*i.e.* quaternary ammonium cations (QACs)) aiming at improving the adsorption capacity towards water pollutants has been also reviewed.<sup>69</sup> Introduction of QACs allows to modify the hydrophobicity of the clay surface and to expand the interlayer space of the 2D materials. Different type of surfactants has been already proposed to this use (*i.e.* organic surfactants with benzyl, phenyl, tetramethylammonium (TMA), trimethylphenylammonium (TMPA), hexadecyltrimethylammonium (HDTMA), cetyltrimethylammonium (CTMA)).<sup>70</sup> The use of Gemini surfactants, characterised by the presence of both aromatic rings and alkyl chain, was also reported for the remediation of water containing pollutants such as bisphenol, p-nitrophenol and triclosan.<sup>71,72</sup>

Very recently, the removal of methylene blue from aqueous solutions has been carried out by using Fe<sub>3</sub>O<sub>4</sub>-multiwalled carbon nanotubes-bentonite composite material.<sup>73</sup>

The anion exchange capacity of clays can be exploited by using physical (*i.e.* thermo-activation processes) and chemical modifications devoted to modifying the interlayer properties of these materials. Chemical activation includes metal or surfactant impregnation and amine grafting. All these methods have, as a general scope, the enrichment of clays surface with positive charges that can be exploitable to interact with anions. The results of these modification methods on nitrate removal have been recently reviewed.<sup>74</sup> Clays modification for the removal of anionic dyes was also recently discussed.<sup>75-76</sup>

Magnetic and mechano-chemical modifications of clays have also been proposed to improve recovery of clays after toxic dyes adsorption and/or to improve their adsorption capacity.<sup>77</sup> In the same review,

Please do not adjust margins



Please do not adjust margins

View Article Online  
DOI: 10.1039/D4DT00757C

the influence of different physico-chemical properties of modified clays (*i.e.* surface area, particles dimensions, morphology, electrical charges, zeta potential, charge density and swelling properties) on the adsorption of synthetic dyes varying several parameters such as pH, ionic strength, dye concentration, contact time, temperature were reported.

Clays treated in acid media and then modified with polymers, surfactants (both anionic and cationic) or materials derived from the combination of clays with magnetic species and polymers and intercalated surfactants and polymers have been proposed for the recovery of heavy metals and inorganic ions, organic dyes, antibiotics, phenolic compounds.<sup>78-80</sup>

Polymer-amended bentonites for application as barriers to limit the contaminants diffusion in solids have been recently reviewed giving particular emphasis on the different type of modification and application fields.<sup>81</sup>

These composite materials have generally excellent impermeability properties that are related to formation of specific bentonite/polymer intercalated and exfoliated structures. Their applicability as a barrier can be exploited in the presence of inorganic salts, heavy metal species and organic contaminants.

Biochar (BC)/ clays composites have been also proposed for the adsorption of adsorption of both inorganic (*i.e.* heavy metals such as Cs, Cr (VI), Zn, nitrates,  $\text{NH}_4^+$ ..) and organic contaminants (*i.e.* dyes, antibiotics, herbicides..) in soil and water.<sup>82</sup>

BCs are very often produced through low-cost methods and have potential capability for environmental contaminants removal. The combination of BC with clays mineral has been therefore proposed in the literature to improve the SSA and thus the adsorption efficiency of BC. These composites can be obtained essentially by using pre-treatment<sup>83</sup> or post-treatment methods.<sup>84</sup> From that reported in the literature it emerges that the synergic combination of clays and BC allow obtaining low-cost materials with better capacities of water and soil remediation respect to the parent constituents because of improved specific surface area and high porosity, chemical, thermal and mechanical stability.

The synthesis step together with physico-chemical properties, data related to toxicity, and regeneration ability of various types of modified clay for environmental purposes have been recently reviewed.<sup>78</sup>

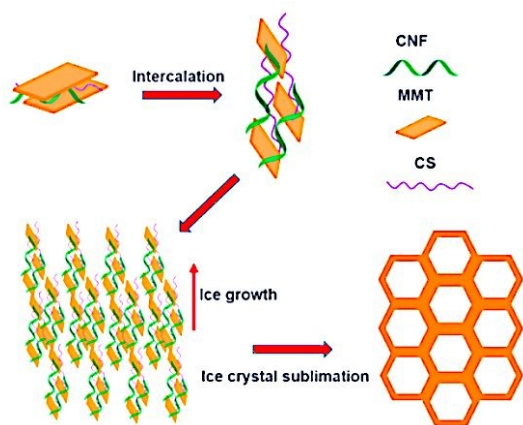


**Fig. 7** Schematic view of the mechanism of the pore structure formation of the MMT-chitosan aerogels. Reproduced with permission from ref. 88, Copyright 2023 Elsevier).

The use of pillared clays for environmental applications also deserves some comments.

Among the different pillaring agents, inorganic ligands such as hydroxo and chloro ligands, metal complex ions with organic ligands and polyhydroxy cations (such as  $\text{AlCl}_3 \cdot 6\text{H}_2\text{O}$ ,  $\text{ZrOCl}_2 \cdot 8\text{H}_2\text{O}$ ) metal ions, metal complexes or neutral particles (such as silica sol particles) are reported. The presence of metal oxide pillars (formed upon calcination step) in the interlamellar space of clays result in a modification of the thermal and hydrothermal stability of clays. The use of pillared clays for environmental applications have been recently reviewed.<sup>85</sup> Applications includes the removal of heavy metals from wastewaters,<sup>86</sup> for the adsorption of VOCs and gas such as methane, ethane, benzene,  $\text{CO}_2$  coming from industrial activities,<sup>87</sup> and for catalytic applications.

Aerogels derived from clays, characterised by porous microstructure, have been proposed in the last decade for their interesting thermal retardant and adsorption properties that are associated with a low toxicity, low cost, and unique structural properties. In particular, montmorillonite (MMT)-based aerogels have been studied to improve their adsorption properties by modifying their preparation method (Fig. 7). A concise review on the possible use of MMT-aerogels for environmental remediation recently appeared in the literature.<sup>88</sup>

## 2.2 Environmental applications of ZrP

Due to the presence of hydroxyl groups with acid properties, ZrP shows a high ion exchange capacity, metal ion selectivity and fast kinetics. Its ability to withstand heat, ionizing radiation, acidic media and an oxidizing environment makes it a very promising material for sorption of radioactive and heavy metal cations.<sup>89,90</sup> Special attention has been given to the removal of  $\text{Cs}^+$  and  $\text{Sr}^{2+}$  cations, because  $^{90}\text{Sr}$  and  $^{137}\text{Cs}$  are present in high level liquid nuclear waste, or highly toxic  $\text{Pb}^{2+}$ ,  $\text{Hg}^{2+}$  and  $\text{Cd}^{2+}$  ions. With the increasing use of rare earth elements in industry in recent times, the need to remove them from contaminated water is also increasing.

The ion exchange capacity of ZrP nanoparticles was found to increase with decreasing particle size.<sup>91</sup> Recently, there were some attempts to affect the  $\text{Sr}^{2+}$  adsorption by changing particle morphology (nanoflowers<sup>92</sup> or spheres<sup>93</sup>) or by surface modification with  $\text{SO}_3\text{H}$  groups.<sup>94</sup> Another approach is based on the use of ZrP derivatives with greater gallery height such are  $\gamma$ -ZrP (for  $\text{Cs}^+$  and rare earths)<sup>95,96</sup>  $\alpha$ - $\text{K}_2\text{Zr}(\text{PO}_4)_2$  (for  $\text{Sr}^{2+}$ ),<sup>97</sup>  $\alpha$ - $\text{Na}_2\text{Zr}(\text{PO}_4)_2 \cdot \text{H}_2\text{O}$  (for heavy metal cations)<sup>98</sup> and  $\alpha$ - $(\text{NH}_4)_2\text{Zr}(\text{PO}_4)_2 \cdot \text{H}_2\text{O}$  (for  $\text{Pb}^{2+}$  and  $\text{Cu}^{2+}$ ).<sup>99</sup> Sorption capacity of ZrP can be enhanced by its combination with organic molecules with high metal affinity. For example, intercalation of 4-amino-benzo-18-crown-6, which has a strong complexing ability for  $\text{Sr}^{2+}$ , into  $\alpha$ -ZrP leads to a composite with excellent stability under acid and radioactive condition and adsorption capacity exceeding



Please do not adjust margins

other similar zirconium adsorbents.<sup>100</sup> Melamine zirconium phosphate<sup>101</sup> synthesized by addition of zirconium tetrachloride to melamine phosphate solution, was tested for absorption of  $\text{Pb}^{2+}$ ,  $\text{Hg}^{2+}$  and  $\text{Cu}^{2+}$ . Sorption ability of  $\gamma$ -ZrP towards rare earth metals can be significantly enhanced by intercalation of p-aminoazobenzene.<sup>102</sup> Clearfield's group reported enhanced ability of mixed zirconium phenylenediphosphonate-phosphate to uptake Nd and Tb cations, where the selectivity for  $\text{Nd}^{3+}$  depends on the amount of phosphate.<sup>103,104</sup>

Graphene oxide-zirconium phosphate nanocomposite, prepared by dropwise addition of zirconium chloride to sonicated graphene oxide suspension, with the subsequent addition of  $\text{NaH}_2\text{PO}_4$ , was tested for the removal of  $\text{Pb}^{2+}$ ,  $\text{Cd}^{2+}$  and  $\text{Cu}^{2+}$  cations.<sup>105</sup>  $\text{Fe}_3\text{O}_4$ @ZrP nanocomposite, prepared by similar way, was efficiently used for  $\text{Hg}^{2+}$  removal from solution.<sup>106</sup> An important benefit of this adsorbent is its simple separation by magnetic power.

Above mentioned adsorbents based on ZrP were tested for metal exchange in batch experiments in a laboratory scale, but these materials are not suitable for column operation in large scale. To overcome this problem, composites with various polymers were tested.  $\alpha$ -ZrP and  $\gamma$ -ZrP encapsulated into mesoporous polystyrene<sup>107</sup> or zirconium phosphate modified polyvinyl alcohol-poly(vinylidene fluoride) membrane<sup>108</sup> demonstrates promising sorption performance for  $\text{Pb}^{2+}$ . Amorphous ZrP nanoparticles exhibit promising adsorption capacity and selectivity for Dy and Nd cations.<sup>109</sup> Recently, the biocomposites of ZrP with cellulose,<sup>110</sup> chitosan,<sup>111</sup> and gelatin<sup>112</sup> were used for sorption of heavy metals. Another elegant way to make ZrP suitable for large scale application is preparation of ZrP monoliths combining micro- and mesopores.<sup>113</sup> All above mentioned examples describe ZrP as a cation adsorbent, but  $\alpha$ -ZrP nanoflakes were also used as a fluoride scavenger. Preferable fluoride adsorption was ascribed to the formation Zr-F complexes.<sup>114</sup>

Another relevant source of environmental pollution are organic dyes. Organic dyes with positive charge or with group that can be protonated and intercalated by zirconium phosphate, but ZrP can also act as a support for species with photocatalytic properties such as titania, silver nanoparticles or graphene oxide and carbon nitrides<sup>90</sup> Rhodamine B was successfully decomposed using zirconium phosphate/silver/silver halide<sup>27</sup> or  $\alpha$ -ZrP carbon nitride composite<sup>115</sup> under ultraviolet light. ZrP-gelatin nanocomposite was able to decompose methylene blue and Fast green under solar light<sup>112</sup> ZrP-chitosan nanocomposite was used for sorption of several type of organic dyes (copper phthalocyanine dye - Reactive blue-21, azo dye Reactive Red 141, and xanthene dye-Rhodamine-6G) and can also serve as a catalyst for a hydrogen peroxide degradation of these dyes.<sup>94</sup>

Co-assembled ZrP nanosheet/1-*n*-butyl-3-methylimidazolium chloride hybrids could serve as highly efficient  $\text{CO}_2$  absorbents.<sup>116</sup>

### 2.3 Environmental applications of LDHs

As known for decades, ion exchange compounds present the properties to trap or release species according to their affinity. Such chemical speciation is often imposed by the charge of the species present. However, the uptake of ions incompatible with the exchanger is possible, as shown by an elegant approach which circumvents the problem of charge compatibility by first intercalating a complexing guest species  $\text{MoS}_4^{2-}$  into LDH with respect to ions of opposite charge such as  $\text{Co}^{2+}$ ,  $\text{Ni}^{2+}$ ,  $\text{Zn}^{2+} < \text{Cd}^{2+} < \text{Pb}^{2+} < \text{Cu}^{2+} < \text{Hg}^{2+} < \text{Ag}^+$  ranked by their selectivity to be removed by the hybrid LDH.<sup>117</sup> Due to its high adsorption capacity, LDH/  $\text{MoS}_4^{2-}$  is very well positioned for the remediation of water polluted by heavy metals. The interlayer species of LDHs may be useful for adsorption of contaminants. It is the case of carboxymethylcellulose (CMC) as interlayer anion to sorb parabens.<sup>118</sup> Interestingly the hybrid CMC LDH can be regenerated at least five times without any pronounced loss of efficiency. LDHs can photo catalytically degrade pollutants such as dyes and nitro-compounds as recently reviewed.<sup>119</sup> Specifically Fenton, photo-Fenton, electro-Fenton reactions are of great interest in advanced oxidation process to decontaminate wastewater, and LDH-based framework including FeMn at cation in their composition compares well with other materials such as spinel-type, perovskite-type or MOF.<sup>120</sup>

In addition to wastewater treatment and the role of LDH as scavenger, some new trends appear concerning  $\text{CO}_2$  photocatalytic reduction<sup>121</sup> and capture to limit the anthropogenic pollution.<sup>122</sup>

To face the new challenge of carbon neutrality, another possibility is to decompose  $\text{CO}_2$  electrocatalytically as it meets the domain of energy as well by producing a renewable fuel.<sup>123</sup> A template based on Cu-Zn-Al LDH is used to form Cu-Zn oxide/Cu-Zn aluminate uniformly dispersed thanks to the cation dispersion within the LDH pristine precursor. An optimised composition is found to reach a Faradaic efficiency of 88.5% for the conversion of  $\text{CO}_2$  to  $\text{C}_2^+$  products. Membranes composed of LDH nanosheets self-assembled with formamidinium sulfonic acid and formed with poly(dimethylsiloxane) are reported to perform greatly for the selective  $\text{CO}_2$  separation.<sup>124</sup>

Shaping of graphene and complementary plasma-assisted oxidation of material open the way to novel devices as efficient membranes for water treatment thanks to optimised diffusion pathway and hydrophilic feature improving the capillary effect for effective water infiltration. That can clearly be considered more as water insertion rather than true intercalation reaction.<sup>125</sup>

Concerning water cleaning, metal/g- $\text{C}_3\text{N}_4$  can display enhanced photocatalytic activity thanks to plasmonic effects in heterostructure with noble metals such as gold and/or platinum. These catalysts can be used for degradation of antibiotic residues and other pharmaceutical contaminants that induce negative environmental effects<sup>126</sup> but it once again consists more in surface reactions than intercalation.

View Article Online

DOI: 10.1039/C4DT00071G

Dalton Transactions Accepted Manuscript



Please do not adjust margins

View Article Online  
DOI: 10.1039/D4DT00757C

## Perspectives

**Table 2.** Most representative examples of intercalation compounds based on clays, ZrP and LDHs for the removal of environmental contaminants. The Reviews are not reported.

| Material  | Preparation   | Mechanism of pollutant removal  | Pollutants removed   | Maximum adsorption Capacity (mg/g)  | Ref |
|---|---|---|--|---|-----|
| Synthetic saponite clays                          | Hydrothermal synthesis followed by Na <sup>+</sup> ion exchange                             | Ion-exchange  | La <sup>3+</sup> , Gd <sup>3+</sup> and Lu <sup>3+</sup>                                     | Gd <sup>3+</sup> : 46.94 ± 1.71<br>La <sup>3+</sup> : 45.21 ± 1.12<br>Lu <sup>3+</sup> : 54.89 ± 1.31<br>From simulated freshwaters:<br>Gd <sup>3+</sup> : 49.48 ± 1.98 | 56  |
| HNTs modified with Fe <sub>2</sub> O <sub>3</sub> | HTNs modified by sol gel method   | electrostatic attraction, ligand exchange, and Lewis acid-base interactions | Phosphate anions   | Maximum ads capacity: 5.46 mg/g   | 62  |
| Fe <sub>2</sub> O <sub>3</sub> /attapulgite       | ultrasonic co-precipitation method  | Adsorption, electrostatic interactions                                      | Arsenite (As <sup>III</sup> )  | ca. 150 mg As(III)/g Fe   | 63  |
| Zero valent iron/kaolin                           | Fe(III) reduction method  | Adsorption, reduction   | Pb(II)   | 440 mg/g  | 64  |
| Zero valent iron/PILC                             | chemical reduction procedure on PILC  | Adsorption, reduction   | nitrates   | -   | 65  |
| Zero valent iron/MMT                              | Impregnation  | Adsorption, reduction   | Pb(II)   | -   | 66  |
| Organo-modified MMT clays                         | Ion exchange  | Adsorption, π-π interaction and hydrophobic affinity                        | bisphenol A  | Maximum adsorption: 222.2 mg/g  | 71  |
| Organo-modified MMT clays                         | Ion exchange with gemini surfactants  | surface adsorption and intraparticle diffusion                              | p-nitrophenol  | 81.30 mg/g (for sample modified with 1,3-bis(dodecyltrimethylammonio)-2-hydroxypropane dichloride (BDHP))   | 72  |
| Fe <sub>3</sub> O <sub>4</sub> -MWCNT-Bentonite   | In-situ growth process  | physical adsorption   | Methylene blue (MB)  | MB adsorption: 48.2 mg/g  | 73  |
| Organo-modified paligorskite and sepiolite        | Grafting process  | adsorption mechanism via hydrophobic interaction and/or hydrogen bonds      | methylene blue (MB) and metanil yellow (MY)  | 60.00 and 59.78 mg/g for grafted sepiolite, for MB and MY, respectively   | 76  |
| Organo-bentonite (AOBent)/sodium (SA) composite   | intercalation of sodium alginate in activated organo-bentonite                              | hydrophobic interactions  | methylene blue (MB) and methyl orange (MO)   | 414 mg/g for MB and 116 mg/g for MO   | 79  |
| Organo-modified acid-treated bentonite            | Acid treatment and ion exchange with surfactants  | surface adsorption and intraparticle diffusion                              | 2,4,5-trichlorophenol (TC)   | TC: 200.6 mg/g  | 80  |
| Organo-modified montmorillonite PILCs             | Grafting process  | ion exchange and coordination interactions                                  | Co <sup>2+</sup> ions  | Co <sup>2+</sup> ions: 60 mg/g  | 86  |
| AlCr-pillared clays                               | One pot hydrothermal methods and ion exchange   | Physical adsorption   | benzene  | Benzene: 48.3 μmol/g  | 87  |
| ZrP nanoparticles                                 | ZrOCl <sub>2</sub> , H <sub>3</sub> PO <sub>4</sub> and aqueous Triton X-100 surfactant     | column separation, ion-exchange   | radioanalytical separation of the no-carrier-added <sup>137m</sup> Ba from <sup>137</sup> Cs | Cs <sup>+</sup> = 2.593 meq/g   | 91  |
| α-ZrP flower-like                                 | ZrOCl <sub>2</sub> , 8H <sub>2</sub> O, Na <sub>3</sub> PO <sub>4</sub> , at 80 °C for 96 h | electrostatic interaction and ion-exchange                                  | <sup>90</sup> Sr from high level liquid waste  | Sr <sup>2+</sup> = 293.43 mg/g  | 92  |
| ZrP-SO <sub>3</sub> H                             | ZrP exfoliation, grafting of  | column separation, surface chemical adsorption                              | <sup>90</sup> Sr from high level liquid waste  | Sr <sup>2+</sup> = 183.21 mg/g  | 94  |

Please do not adjust margins





Please do not adjust margins

|  | (3-Mercaptopropyl)tri methoxysilane, oxidation   |  |   | View Article Online<br>DOI: 10.1039/D4DT00757C   |             |
|--|--|--|---|--|-------------|
| $\gamma$ -ZrP  | -  | ion-exchange   | rare earth metal cations  | 0.06–0.10 mol per mol of $\gamma$ -ZrP   | 95          |
| $\gamma$ -ZrP  | ZrOCl <sub>2</sub> ·8H <sub>2</sub> O, NaH <sub>2</sub> PO <sub>4</sub> ·H <sub>2</sub> O and NaF grounded in an agate mortar, 120 °C for different times                                      | ion-exchange   | Selective adsorption of Cs <sup>+</sup>   | Cs <sup>+</sup> removal efficiency >98%  | 96          |
| K <sub>2</sub> Zr(PO <sub>4</sub> ) <sub>2</sub>                               | solid state reaction using ZrO <sub>2</sub> and KPO <sub>3</sub> (750 °C for 24 h)   | ion-exchange   | Separation of <sup>90</sup> Sr from nuclear waste   | Sr <sup>2+</sup> = 603 $\mu$ mol/g   | 97          |
| Zr(NaPO <sub>4</sub> ) <sub>2</sub> ·H <sub>2</sub> O                          | ZrOCl <sub>2</sub> ·8H <sub>2</sub> O, Na <sub>2</sub> HPO <sub>4</sub> and NaF were ground in an agate mortar. Heated to 120 °C for 24 h.   | ion-exchange   | heavy metals such as Pb <sup>2+</sup> , Cu <sup>2+</sup> , Cd <sup>2+</sup> , and Tl <sup>+</sup> | highly toxic Tl <sup>+</sup> = 1036 mg/g   | 98          |
| $\alpha$ -Zr-(NH <sub>4</sub> PO <sub>4</sub> ) <sub>2</sub> ·H <sub>2</sub> O | ZrOCl <sub>2</sub> ·8H <sub>2</sub> O, (NH <sub>4</sub> ) <sub>2</sub> HPO <sub>4</sub> and NaF were ground in an agate mortar. Heated to 120 °C for 24 h.                                     | ion-exchange   | Pb <sup>2+</sup> and Cu <sup>2+</sup>   | Pb <sup>2+</sup> = 398 mg/g<br>Cu <sup>2+</sup> = 144 mg/g   | 99          |
| AM-ZrP<br>AM=4-amino-benzo-18 crown 6  | intercalation of AM in $\alpha$ -ZrP preintercalated with butylamine   | complexation by AM   | <sup>90</sup> Sr generated in the nuclear fuel cycle  | Sr <sup>2+</sup> = 320.16 mg/g   | 100         |
| M-ZrP<br>M=melamine  | preparation of melamine phosphate (MP). Precipitation reaction between MP and ZrCl <sub>4</sub> to obtain M-ZrP  | chelation by M   | Pb <sup>2+</sup>  | Pb <sup>2+</sup> = 1000 mg/g   | 101         |
| $\gamma$ -ZrP-p-aminoazobenzene  | intercalation of the azo compounds into $\gamma$ -ZrP  | Ion-exchange and complexation by p-aminoazobenzene                       | lanthanoid elements   | lanthanoid elements = 370 mg/L on average  | 102         |
| zirconium phenylenediphosphonate-phosphate                                     | Hydrothermal synthesis (120 °C for 4 days) of ZrOCl <sub>2</sub> ·8H <sub>2</sub> O, C <sub>6</sub> H <sub>4</sub> (PO <sub>3</sub> H <sub>2</sub> ) <sub>2</sub> and phosphoric acid solution | Ion-exchange   | Nd <sup>3+</sup> , Tb <sup>3+</sup>   | Nd <sup>3+</sup> = 99% of uptake<br>Tb <sup>3+</sup> = 98% of uptake   | 103,<br>104 |
| GO-Zr-P  | addition of zirconium chloride to the GO suspension under sonication   | chemisorption, mainly through surface complexation                       | Pb <sup>2+</sup> , Cd <sup>2+</sup> , Cu <sup>2+</sup> , Zn <sup>2+</sup>                         | Pb <sup>2+</sup> = 363.42 mg/g<br>Cd <sup>2+</sup> = 232.36 mg/g<br>Cu <sup>2+</sup> = 328.56 mg/g<br>Zn <sup>2+</sup> = 251.58 mg/g | 105         |
| Fe <sub>3</sub> O <sub>4</sub> @ZrP  | ZrOCl <sub>2</sub> ·(NH <sub>4</sub> ) <sub>2</sub> HPO <sub>4</sub> , sodium lauryl sulphate and Fe <sub>3</sub> O <sub>4</sub> nanoparticles were stirred for 3 h at room temperature        | chemical adsorption  | Hg <sup>2+</sup>  | Hg <sup>2+</sup> = 181.8 mg/g  | 106         |
| ZrP@MPS<br>MPS= mesoporous polystyrene   | MPS was immersed into ethanol solutions containing ZrOCl <sub>2</sub> , followed by evaporation. The beads were incubated with H <sub>3</sub> PO <sub>4</sub> for 24                           | highly specific inner-sphere coordination of nanoconfined $\gamma$ -ZrP, | Pb <sup>2+</sup>  | Pb <sup>2+</sup> = 180 mg/g  | 107         |



Please do not adjust margins

| Please do not adjust margins   |   |  |   |   |     |
|--|---|--|---|---|-----|
| PVA/ZrP PVDF membrane  | PVA and zirconium ions could be coated onto the PVDF membrane through crosslinking reactions with glutaraldehyde. The Zr/PVA modified membrane was immersed into the phosphate solution | ion exchange   | Pb <sup>2+</sup>  | Pb <sup>2+</sup> = 121.2 mg/g   | 108 |
| amorphous-ZrP  | solutions of ZrCl <sub>4</sub> and H <sub>3</sub> PO <sub>4</sub> were mixed, the precipitated solid was allowed to stand over night  | ion exchange   | Nd <sup>3+</sup> , Dy <sup>3+</sup>   | Nd <sup>3+</sup> = 0.610 meq/g<br>Dy <sup>3+</sup> = 0.628 meq/g  | 109 |
| hydrophilic cellulose- $\alpha$ -ZrP                                   | Dispersion of nano-sized $\alpha$ -ZrP was sprayed onto the surface of the pure cellulose membranes under vacuum filtration   | electrostatic attraction between the heavy metal ions and the high-negatively charged membrane's surface, ion exchange | Pb <sup>2+</sup> , Ni <sup>2+</sup> , Cu <sup>2+</sup> , Zn <sup>2+</sup>   | Cu <sup>2+</sup> , Zn <sup>2+</sup> , Ni <sup>2+</sup> , Pb <sup>2+</sup> = removal efficiency of 97.0, 98.0, 99.5, and 91.5%, respectively | 110 |
| chitosan-ZrP   | Chitosan and ZrP solution was mixed and kept in stirring condition for 24 h   | Electrostatic interactions   | Cr <sup>6+</sup> , Reactive blue-21 (RB-21), Reactive Red 141 (RR-141), Rhodamine-6G (Rh-6G)  | Cr <sup>6+</sup> = 311.53 mg/g<br>RB-21 = 457 mg/g<br>RR-141 = 435.1 mg/g<br>Rh-6G = 438.6 mg/g   | 111 |
| Gelatin-ZrP  | sol-gel method  | ion exchange   | Selective adsorption of Cd <sup>2+</sup>  | Cd <sup>2+</sup> removal efficiency >96%  | 112 |
| ZrP monolith   | ZrOCl <sub>2</sub> ·6H <sub>2</sub> O, HCl, glycerol, poly(ethylene glycol), polyacrylamide, H <sub>3</sub> PO <sub>4</sub>   | electrostatic interactions   | adsorption of Ag <sup>+</sup> , Cs <sup>+</sup> , Sr <sup>2+</sup> , Zn <sup>2+</sup> , Cu <sup>2+</sup> , Pb <sup>2+</sup> , Cd <sup>2+</sup> , Fe <sup>3+</sup> | Percentage of all cations adsorption % >92%   | 113 |
| ZrP nanoflake  | ZrOCl <sub>2</sub> in ethanol, HCl, H <sub>3</sub> PO <sub>4</sub> , stirred thoroughly for 24 h at 60°C  | strong inner-sphere complexation achieved by Zr-F bonds  | fluoride scavenging   | F = 55.7 mg/g   | 114 |
| C <sub>3</sub> N <sub>4</sub> -ZrP                                     | $\alpha$ -ZrP nanoparticles and C <sub>3</sub> N <sub>4</sub> colloid was dispersed in deionized water and ultrasonicated. The mixture was stirred at 80 °C for 3 h                     | photodegradation   | RhB   | RhB degradation efficiency = 99.95%   | 115 |
| ZrP /BMIMCl<br>BMIMCl = 1-n-butyl-3-methylimidazolium chloride hybrids | Exfoliated ZrP was acid treated mixed with BMIMCl under ultrasonication   | Physical and chemical absorption   | CO <sub>2</sub>   | CO <sub>2</sub> capture capacities = 0.73 mmol/g at 60 °C   | 116 |
| MgAl-MoS <sub>4</sub> -LDH   | (MoS <sub>4</sub> ) <sup>2-</sup> was intercalated in MgAl-NO <sub>3</sub> via ion exchange reaction  | chemisorption with the adsorption mechanism via M-S bonding  | selective removal of Cu <sup>2+</sup> , Pb <sup>2+</sup> , Ag <sup>+</sup> , and Hg <sup>2+</sup>   | Hg <sup>2+</sup> = 500 mg/g<br>Ag <sup>+</sup> = 450 mg/g   | 117 |
| MgAl-CMC<br>CMC = carboxymethylcellulose                               | coprecipitation at low supersaturation of LDH in presence of CMC  | chemisorption  | 4-methyl-, 4-propyl- and 4-benzylparaben  | 4-methylparaben = adsorption capacity >70%  | 118 |
| Cu-Zn oxide/Cu-Zn aluminate  | CuZnAl-LDH decomposed to CuZn oxide/CuZn aluminate pre-catalyst. Electrochemical  | Electrochemical CO <sub>2</sub> reduction reaction   | CO <sub>2</sub>   | Faradaic efficiency of 88.5% for the conversion of CO <sub>2</sub> to C <sub>2</sub> products   | 123 |

View Article Online  
DOI: 10.1039/D4DT00757C

Dalton Transactions Accepted Manuscript



Please do not adjust margins

|  | reduction to generates CuZn alloy                                    |   |  | View Article Online<br>DOI: 10.1039/D4DT00757C                                     |     |
|--|--|---|--|--|-----|
| (LDH/FAS) <sub>n</sub> -PDMS<br>FAS= formamide sulfonic acid<br>PDMS= poly(dimethylsiloxane) | self-assembly of LDH, FAS, followed by spray-coating with PDMS layer | synergy of enhanced solubility, diffusivity and chemical affinity for CO <sub>2</sub> in the sub-nanometre channels | separation of CO <sub>2</sub>  | Maximum CO <sub>2</sub> selectivity factor (CO <sub>2</sub> /CH <sub>4</sub> ): 62 | 124 |
| vertically aligned graphene sheets membran   | antifreeze-assisted freezing technique                               | solar thermal purification  | Cr <sup>3+</sup> , Pb <sup>2+</sup> , Zn <sup>2+</sup> , Ni <sup>2+</sup> , Cu <sup>2+</sup> | removal efficiency 99.5%   | 125 |
| Au/Pt/g-C <sub>3</sub> N <sub>4</sub>  | calcination-photodeposition technique                                | plasmonic photocatalys  | tetracycline hydrochloride (TC)  | 93.0% of TC degraded in 3 h  | 126 |

### 3. Applications of intercalation materials for health purposes

Intercalation compounds are more and more studied regarding their possible application in health domain. Once their biocompatibility has been verified, it is indeed possible to consider inorganic structures that can provide solutions, for the release of active ingredients, for antimicrobial or bone reconstruction activity, or even more generally for theranostic applications as reviewed recently.<sup>127,128</sup>

Representative applications of intercalation compounds based on clays, ZrP and LDHs for health purposes are described below and then summarised in Table 3.

#### 3.1 Applications of clays in the health domain

Nanoclays are attracting increasing interest for their enhanced therapeutic effects. Indeed, their biocompatibility, the bacteriostatic or bactericidal activity exhibited by some clays<sup>129</sup> as well as their high surface area, adsorption capacity, ability to serve as carrier for therapeutic and to release drugs in a controlled manner make them ideal candidates for applications in biomedical engineering<sup>130</sup>, tissue engineering and regenerative medicine<sup>131</sup>, wound healing<sup>132</sup>, drug delivery systems<sup>133</sup> bioimaging<sup>134</sup> and 3D bio inks for use in medical purposes.<sup>135</sup> It is worthy to note that not attention has also been paid to commercially available clays such as Laponite® in the field of health as reviewed by Tomas et al.<sup>136</sup> owing to their purity but above all due to their high aspect ratio derived from their 25 nm disk-shaped particles. The most promising use of clays and clay-based nanocomposite is in the field of drug delivery systems<sup>137-141</sup>, including antimicrobial<sup>142,143</sup> antibiotic<sup>143,144</sup>, anti-cancer<sup>145</sup> as well as theranostics<sup>146,147</sup> and antihistamines treatments.<sup>148</sup>

Montmorillonite (MMT) clay has been frequently utilized as drug vehicles due to its high specific surface area, excellent cation exchange capacity and biocompatibility. To avoid flocculation of MMT under physiological conditions the surface has to be modified. As a matter of example, PEGylated chitosan (PEG-CS) adducts can be used to modify the clay surface thus leading to a good dispersion in serum-containing environment (Fig. 8) as well as resulting in interesting drug carriers.<sup>145</sup>

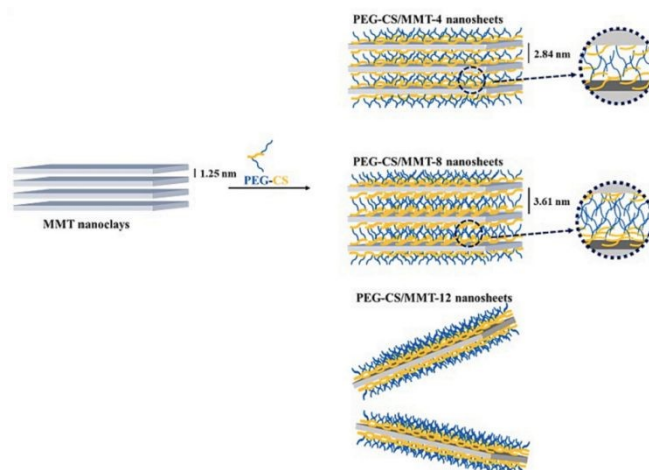


**Fig. 8** microstructures of PEG-CS/MMT nanosheets with various PEG-CS/MMT. Reproduced with permission from ref. 145, Copyright 2022 Elsevier.

Examples of the uses of PCHs derived from MMT clays for drug delivery applications are also reported. PCHs prepared using montmorillonite as starting material are interesting supports for methotrexate MTX encapsulation due to the superior drug encapsulation efficiency (EE) respect to MMT parent clay (EE values higher than 97% for PCHs compared to EE = 45% for MMT clay).<sup>134</sup> It was also observed that PCHs hosts can influence the drug release in relation to their pore architecture. The release proportion of drug is released in a proportion higher than 70% whereas from MMT parent clay MTX is released only 9.7%.<sup>134</sup>

Halloysite is one of clay minerals showing maximum efficiency as a nano drug carrier and demonstrates exceptional biocompatibility and low cytotoxicity when tested for use in cell cultures and tissues.<sup>149,150</sup> Moreover, thanks to its size, the inner lumen can accommodate molecules of interest while small drug molecules can be filled in the wall interlayer spaces and molecules can be either adsorbed covalently bounded on the outer surface. As different interactions can occur, an initial drug burst can start from the outer surface and be followed by a sustained release of the drug from the inner surface (lumens) owing to a slower leakage.

Drugs can be loaded into HNTs from saturated drug solutions or a melt of low water-soluble drugs. Pan et al.<sup>151</sup> loaded vancomycin, a drug used for serious Gram-positive bacterial infections, into the



Please do not adjust margins

internal cavity of halloysite by using different mass ratios of Vancomycin and halloysite via sonication and vacuuming obtaining a solid with high antibacterial activity to *S. aureus* and *B. streptococcus*. The exploitation of HNTs allowed the preparation of local antibiotic delivery system without the need of particular energy-consuming process, thus allowing the controlled release of molecules beneficial for targeted applications.

Norfloxacin, an anti-microbial agent was loaded within HNT and then embedded with chitosan to prepare bio-nanocomposite films.<sup>152</sup>

Antimicrobial gelatin-based elastomer nanocomposites membranes loaded with ciprofloxacin and polymyxin B sulfate loaded-halloysite nanotubes were formed for wound dressing applications.<sup>153</sup> Combining ciprofloxacin (characterised by a broad-spectrum antimicrobial activity inhibiting both Gram-negative and Gram-positive bacteria) and polymyxin B-sulfate having a narrow spectrum of activity mainly against Gram-negative aimed at having a co-operative anti-infection effect. It was reported that HTNs has a dual role of enhancing the matrix tensile strength and slowing down the release rate of high dissoluble drug.

Recently, the formation of a hybrid system based on biocompatible poly 2-hydroxyethyl methacrylate (PHEMA) and thymol-loaded halloysite was reported for application as portable wound dressing to protect injured skin<sup>154</sup>, the antibacterial, antifungal anti-inflammatory, properties of thymol make this compound interesting for the development of devices for tissue repair. Also in this case, HTNs was exploited to entrap the thymol into the lumen to ensure a sustained release of the drug.

Doxorubicin (DOX) is widely used as a chemotherapeutic drug, owing to its effectiveness in combating numerous types of cancers. However, as some serious side effects have been witnessed, DOX delivery vectors based on different host were developed as recently reported.<sup>155</sup> In this frame, DOX was for example loaded into HNTs and then encapsulated by soybean phospholipid (LIP) to form HNTs/DOX/LIP.<sup>156</sup> The optimal DOX loading efficiency was higher than 22 %. A pH-responsive release property with fast drug release under acidic conditions (pH =5.4) was evidenced by in vitro drug release test and in vivo experimental results revealed that such compounds exhibit a significantly higher inhibitory efficacy on the growth of mouse gastric cancer cells than free DOX at the same drug concentration.

The development of chitosan/halloysite/graphitic-carbon nitride compounds for quercetin targeted delivery was performed to overcome the weak hydrophilicity, chemically unstable and low bioavailability of quercetin, which presents on the other side, anti-inflammatory, antiviral and mainly anticancer effects. The combination of carbon nitride ( $g\text{-C}_3\text{N}_4$ ) which is similar in structure with graphene, has a low biological toxicity and can be metabolised in biological systems<sup>157</sup> with HNT and chitosan to form hydrogels followed by a loading of quercetin using a water in oil in water emulsification process to attain quercetin sustained-release lead to a remarkable encapsulation loading and loading efficiency (up to 86%), the formation of a pH-responsive behaviour minimizing the side effect of quercetin by controlling its burst release at neutral conditions. These new nanocomposites revealed also a significantly

higher cytotoxicity against breast cancer cells in comparison to quercetin as a free drug.

View Article Online  
DOI: 10.1039/D4DT00757C

The reported examples suggested that clays can be exploited as nano containers for applications in drug delivery, antimicrobial materials, self-healing polymeric composites, and regenerative medicine that entail time-extended functions.

In the field of tissue engineering, which aims to develop biological substitutes that replace, restore, structural and functional properties of tissues, HNTs are also arguably the most perspective candidates as beside all there already mentioned properties, their unique structure can significantly increase the mechanical and chemical stability of tissue engineering scaffolds.<sup>158-160</sup> Applications for bone tissues<sup>161</sup> cartilage repair<sup>162</sup>, implants,<sup>163</sup> dental fillings,<sup>164</sup> and tissue scaffolds<sup>165</sup> underlined all the advantages of HNTs. As interesting results, in the field of orthopedic implants, Dharmaraj et al.<sup>163</sup> mentioned the antibacterial, anti-cancer and osteosarcoma cell growth impediment of composites prepared by electrodeposition of strontium-halloysite nanotubes (Sr-HNT)/lanthanum, cerium substituted hydroxyapatite composite coatings on titanium used as implant materials. In addition, an anti-corrosion effect of this new type of coating was also revealed. 3D-printed scaffold with a sequential delivery platform was also formed starting from deferoxamine loaded HTNs, bone morphogenetic protein-2 and poly (L-lactide-co-glycolide)/b-tricalcium phosphate solution with the aim of realizing the coupling regeneration of blood vessels and bones.<sup>165</sup> These new composites promote cell-scaffold interactions by enabling cell adhesion, spreading, and differentiation in vitro, and enhance also subcutaneous ectopic bone formation in vivo via the synergistic effect of deferoxamine and bone morphogenetic protein-2 paving therefore the way of new treatments for bone defects.

The inherent properties of clay minerals, such as fluorescence and paramagnetism, enable their utilization in biomedical imaging techniques. Functionalised clay nanoparticles have been developed as contrast agents for magnetic resonance imaging (MRI), providing improved imaging resolution and targeting capabilities. Paramagnetic clays have been obtained by introducing in the interlayer space of saponite clays  $\text{Gd}^{3+}$ -complexes by a classical ion exchange reaction. It was pointed out that the interactions of the complexes with the saponite layers have a peculiar influence on both the local rotational dynamics and exchange process of water molecules between the internal  $\text{Gd}^{3+}$  coordination sphere and the bulk.<sup>166,167</sup> Clay-based lanthanide polymer nanocomposites were for example formed<sup>135</sup>, starting from polyethyleneimine and a lanthanide complex attached onto the surface of halloysite or palygorskite leading to nanocomposites exhibiting both intense red emission under visible light excitation, long luminescent lifetime as well as high quantum yields, and improved photoluminescence stability. The photoluminescent and magnetic properties of multifunctional halloysite nanotube  $\text{Fe}_3\text{O}_4$ @HNT-polyethyleneimine-Tip-Eu(dibenzoylmethane)<sub>3</sub> were also reported<sup>168</sup> one interesting feature being that these composites displayed superparamagnetic behaviour and also worked as a magnetic resonance imaging (MRI)



Please do not adjust margins

contrast agent in vitro and in vivo. The Schikorr reaction, which involves the oxidation of layered  $\text{Fe}(\text{OH})_2$  was used to prepare superparamagnetic  $\text{Fe}_3\text{O}_4$  – Laponite.<sup>169</sup>

### 3.2 ZrP-based compounds for health applications

The discovery that ZrP is harmless to the body, since it is highly hemocompatible, not toxic, and not associated with any metabolic function, have paved the way for using these compounds in the nanomedicine field.<sup>170</sup> The insertion in ZrP of molecules of biological interest can occur via ion-exchange reactions between the acid protons of the solid and the molecular cations, intercalation of basic molecules and topotactic exchange of phosphate by phosphonate groups. The last strategy is mainly applied in the  $\gamma$ -ZrP. In this context, the alendronate, a gem-bisphosphonate used to treat bone diseases, was immobilized in  $\gamma$ -ZrP by topotactic exchange to obtain a drug delivery system.<sup>171</sup> When the biological molecules are particularly bulky a preintercalation step in alpha type is mandatory to enlarge the interlayer region; a strategy to avoid this step is the use of  $\theta$ -ZrP, an hydrated form of  $\alpha$ -ZrP with six water molecules per formula unit. Otherwise, one-pot intercalation can be achievable by starting from a gel of nanometric  $\alpha$ -ZrP in ethanol or propanol.<sup>172</sup> The alcohol present in the interlayer region keeps the layers far enough apart to promote the intercalation of bulky species.

Particular attention has been paid to delivering chemotherapeutic drugs loaded in nanocarriers, to target cancer cells and minimize their side-effects. DOX, one of the most used anticancer drugs, is highly toxic to cancer cells and to normal tissue causing several adverse effects. To overcome these drawbacks, DOX was intercalated into  $\theta$ -ZrP to obtain a compound ( $\text{DOX@ZrP}$ ) with a drug loading of 34.9 wt%. Two dimensional <sup>31</sup>P NMR studies showed that DOX is intercalated as a neutral molecule and interacts with the ZrP layers by hydrogen bonds among protonated phosphate groups and the amine and -OH groups of DOX, involving also hydration water molecules. The release of DOX from  $\text{DOX@ZrP}$  in simulated body fluid at pH 7.42 is prolonged, extending until 11–14 days. Cellular studies showed that the samples  $\text{DOX@ZrP}$  favoured the cellular uptake and cytotoxicity in MCF-7 and MDA-MB 231 cancer cell lines compared with free DOX. In vitro studies in MCF-7 and MCF-10A cells showed that ZrP nanoparticles are able to promote the uptake of  $\text{DOX@ZrP}$  by endocytosis especially in cancerous cells.<sup>173</sup> The biocompatibility of the  $\text{DOX@ZrP}$  was improved by the surface functionalisation with monomethyl-poly(ethylene glycol)-monophosphate and cytotoxicity towards human prostate cancer PC3 cells was about 20% higher than free DOX.<sup>174</sup>

Kalita et al. prepared nanometric zirconium pyrophosphate, having dimension of about 48 nm, by sonochemical method in presence of cetyltrimethylammonium bromide as surfactant followed by calcination at 700°C. The nanoparticles were used to immobilize curcumin ((1E,6E)-1,7-Bis(4-hydroxy-3-methoxyphenyl)-1,6-heptadiene-3,5-dione), a model drug with anti-inflammatory, antioxidant and anti-tumour properties. The loading of the drug in the composite (ZP-CUR) was 11.5% wt. The in vitro drug release from

ZP-CUR was pH sensitive and was higher at pH 5 than pH 7.4 making the composite suitable to deliver and release the drug in the acidic intracellular environment of the tumor cells. The cytotoxicity studies of free curcumin and of ZP-CUR, performed on MDA-MB-231 breast cancer cell lines, showed an enhancement of the cytotoxic effect of the formulate curcumin as compared to the native form.<sup>175</sup>

The antitumor drugs lack specificity for tumor cells exhibiting thus high cytotoxicity also for normal cells. The use of magnetic nanoparticles ( $\text{Fe}_3\text{O}_4$ ), anchored to the nanocarrier, allows, through an external magnetic field, to deliver and anchor the drug in a specific site enhancing the drug activity. In this context, Kalita et al. extended their work with curcumin-loaded amorphous zirconium phosphate as the shell for magnetite core nanocarriers.<sup>176</sup> The release profile, cytotoxicity on MDA-MB-231 cell lines was comparable with those of ZP-CUR previously described.

To improve targeted drug delivery to tumour cells, nanocarriers conjugated with folate seem to be a promising strategy since the cancer cells over-express folate receptors. Magnetite nanoparticles and 5-fluorouracil (5-FU) were intercalated in  $\alpha$ -ZrP preintercalated with butylamine. The compound obtained was covered by a folate acid–chitosan–rhodamine6G (FA-CHI-R6G) complex to obtain the system 5-FU/ $\text{Fe}_3\text{O}_4$ / $\alpha$ -ZrP@FA-CHI-R6G (Fig. 9). The presence of R6G, that acts as a fluorescent probe, candidates the nanocomposite as a promising material for bioimaging. Moreover, the nanocomposite has no cytotoxic effects on A549 cells, interacts with FA positive HeLa cells while the FA negative HEK293 cells show little uptake of the nanomaterials, and shows a sustainable 5-FU release.<sup>177</sup>

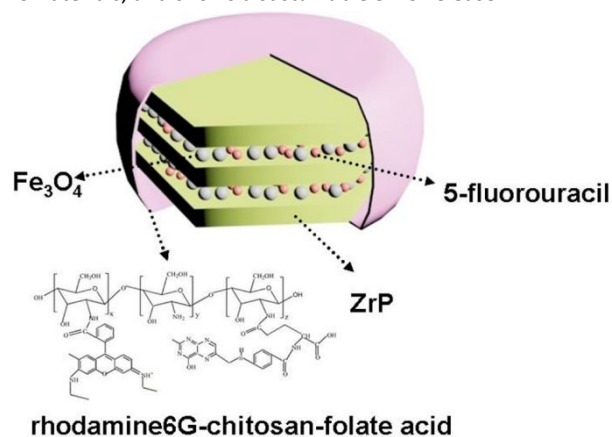


**Fig. 9** Schematic representation of the 5-FU/ $\text{Fe}_3\text{O}_4$ / $\alpha$ -ZrP@CHI-FA-R6G Nanocomposites. Reproduced with permission from ref 177. Copyright 2015 American Chemical Society.

An alternative to the use of chemotherapeutic drugs for the cancer treatment is the photodynamic therapy (PDT) that is based on photo activation of a photosensitizer able to form cytotoxic reactive oxygen species. The photosensitizers, as the antitumor drugs, have nonspecific interactions causing damage also to normal cells.

The photosensitizer methylene blue (MB) was intercalated in  $\alpha$ -ZrP by cation exchange with the acid protons. The ZrP-MB nanoparticles were able to deliver MB to MDA-MB-231 breast cancer cells and to reduce the toxicity of pure MB in the dark experiment. PDT efficacy



Please do not adjust margins

on ZrP-MB treated MDA-MB-231 cells was enhanced upon MB intercalation. The nanoparticles protect the MB from the reduction to "leuco-methylene blue" in biological systems, that generally limit the clinical use of MB, and release it preferentially in the cancer cells due to their acidic microenvironment.<sup>178</sup>

Several active molecules were intercalated starting from the gel of nanometric  $\alpha$ -ZrP in ethanol. Chlorhexidine (CLX), a broad spectrum antimicrobial agent, was intercalated starting from the gel of nanometric  $\alpha$ -ZrP reaching a drug loading 50 %wt. ZrP(CLX) was used as filler of sodium carboxymethylcellulose to prepare films as potential wound dressings. The films showed antimicrobial and antibiofilm activity. Moreover, in vitro cytotoxicity tests of the films in HDF human dermal fibroblast cells (HuDe) and human keratinocyte cell lines (NCTC2544) showed reduced cytotoxicity of CLX due to its prolonged release, which maintains low CLX concentration.<sup>179</sup> Silver NPs were immobilized on  $\alpha$ -ZrP via  $H^+/Ag^+$  ion-exchange process followed by thermal treatment. The Ag-enriched  $\alpha$ -ZrP showed antimicrobial activity against *Escherichia coli*.<sup>180</sup>

The intercalation properties of the gel of nanometric  $\alpha$ -ZrP in ethanol were exploited to intercalate potent in-house *S. aureus* NorA efflux pump inhibitors. The intercalation compounds were used as filler of poly(lactide-co-glycolic acid). The composites showed an antibiofilm activity comparable to that of film containing ZrP intercalated with thioridazine, a NorA and biofilm inhibitor.<sup>181</sup>

An alternative way to promote the interactions between the  $\alpha$ -ZrP surface and biomolecules is the use of gel of zirconium phosphate obtained by exfoliation with propylamine and regenerated with HCl. The gel was able to immobilize the anti-inflammatory drug bromfenac (BFS)<sup>182</sup> and caffeine,<sup>183</sup> a central nervous system stimulant. The compound ZrP-BFS showed a BFS release profile pH dependent; a complete release of BFS was obtained at pH 7.

Finally, ZrP-gentamicin intercalation compound was used as filler of a thermoplastic polymer and the composite was processed via high temperature melt extrusion into 3D scaffolds. The antibiotic, released in sustained manner, maintain its activity against Gram + and Gram - bacterial and the scaffolds was no cytotoxic towards hMSCs cells and it no prevented their osteogenic differentiation.<sup>184</sup>

### 3.3 Applications of LDHs for health purposes

LDHs are also studied today for their possible biomedical applications.<sup>185</sup> Their trapping and release ability is concerned regarding the delivery of drugs or bioactive molecule as well as their easiness to be handled and scaled-up.<sup>186</sup> Accommodation of bioactive molecules within LDH host structure leads to bioactive hybrid materials that can be efficient in administration associated to low cytotoxicity, this triggered by pH human fluids to target precise site. They may be of use to deliver cosmeceutical natural or synthetic biomolecules. When considering the formed bio-hybrid composite, it may be considered as a winning-winning partnership, the host LDH protecting the bioactive molecule from aggressive medium while the guest maintains the layered structure together until its ingress out

the LDH cargo. Due to their biocompatibility, LDHs are also studied to address in terms of clinical translation their bio-activity and bio-reactivity concerning orthopaedic diseases and other bone tumours.<sup>187</sup>

LDH supported MOF loaded in alginate beads, a pH-sensitive biopolymer extracted from seaweed,<sup>188</sup> is prepared to control the release of DOX for cancer therapy. In vitro cytotoxicity on MCF-7 cells (human breast cancer cells) showed that the loaded beads have a higher cytotoxic effect than the free DOX. The higher DOX activity may be due to the presence of Alg coating and controlled DOX release into cancer cells. Other reviews report the combination of organic polymer with LDH as well.<sup>189</sup> Form in vivo assays, it is demonstrated that such bio-hybrid composites embarking bioactive guests are of interest in pharmaceutical and medical applications, and in that review more specifically focused on drug delivery and tissue engineering regarding skin and bone therapies. For the latter, it is observed that LDH composites can be safely integrated to living matter as well as being stimuli-response when exposed to collagen. Of course, other clay minerals naturally occurring such as montmorillonite and halloysite may be also combined with biocompatible polymers to embark active ingredient of interest in drug delivery or in tissue engineering.<sup>190</sup> In the latter case, the bio-hybrid composites are found to induce cell adhesion and their proliferation helping in regenerating skin damage. It is indeed the set of 2Ds materials which can be considered as bio-platforms in theragnostic (therapeutic and diagnostic) when endowed with bio-functionalities,<sup>191</sup> as found in the critical and cutting-edge review discussing the current challenges and their future research directions regarding such application in human health.

Chemo-therapeutic and gene-therapeutic functions for hetero-structured layered nanohybrids using clays (in general) are recently reviewed, underlining the possibility of drug-clay nanohybrid to be relevant for the drug administration and release.<sup>192</sup>

Similarly, another review reports such carriers on gene-LDH focusing on intercellular gene uptake mechanisms and their intracellular ingress but also with imaging and targeting functions.<sup>193</sup>

Other health domains may be concerned such as tissue and bone engineering where LDH dispersed into fibers of poly (epsilon-caprolactone) (PCL) by electrospinning technique are studied to mimic tissue-engineering scaffolds.<sup>194</sup> The study reports the viability, proliferation, and adipogenic differentiation of mouse adipose derived stem cells and shows that LDH-enriched electrospun PCL scaffolds with high porosity increase cell adhesion and proliferation suitable for application in soft tissue regeneration.

More specifically for bone healing, 3D additive manufactured scaffolds made with biodegradable polymers and LDH intercalated with ciprofloxacin are designed to present possible antibiotics release for an antimicrobial activity to prevent infection in the case of an open bone fracture or implant surgery. Incorporation of LDH-ciprofloxacin into the scaffolds did not affect the viability of human mesenchymal stromal cells (hMSCs) or prevent their osteogenic differentiation.<sup>184</sup> Intercalation/exfoliation procedure following Hummer's method led to the synthesis of graphene oxide (GO). Consecutively to this intercalation process, the so-obtained materials



Please do not adjust margins

exhibit a size-dependency of GO antimicrobial activity. The defect quantity is correlated to the size/specific surface of the GO, giving guidelines for future development of graphene-based antimicrobial surface coatings.<sup>195</sup>

Tunable surface properties, transparency, electronic capabilities, biocompatibility and outstanding flexible mechanical properties make graphene a promising material for biomedical applications such as biomedical electronic devices or implants. However, the generally called “graphene” material results in fact in a large variety

of carbon-based materials. Following these considerations, graphene-based materials used for biomedical applications must be regarded by paying particular attention to the characterizations defining it. Consequently, some “rules” must be established concerning the synthesis considerations and the possible biomedical applications depending on the characteristics of graphene. If graphene can be obtained by CVD procedure, intercalation using Hummer’s method can lead to GO and then Reduced Graphene Oxide (RGO) interesting for health’s purpose.<sup>196</sup>

**Table 3.** Most representative examples of intercalation compounds based on clays, ZrP, LDHs and graphene for health purposes. The data contained in reviews are not reported.

| Material/substrate                             | Active specie  | Procedure to introduce the active species  | Application   | Biological system  | Ref. |
|--|--|--|---|--|------|
| Palygorskite and HNTs clays                    | Eu(DBM) <sub>3</sub> (H <sub>2</sub> O) <sub>2</sub> (HDBM dibenzoylmethane) | PEI grafting and further modification with terpyridine derivatives to introduce an antenna species. The Eu complex is introduced via a ligand exchange reaction. | bioimaging applications   | Tested for bioimaging with HeLa cell line. Promising in applications as targeting cancer cells and in drug delivery systems                | 134  |
| Amino-modified clays in liposomes              | budesonide   | polyelectrolytes, aminoclay and Eudragit® S100, were assembled directly on the liposomal surface via a layer by layer deposition                                 | drug releasing carriers   | Colon-targeted delivery system   | 138  |
| Porous clay heterostructures based on MMT clay | methotrexate (MTX)   | MTX encapsulation  | MTX delivery systems, chemotherapy  | Potential use of PCHs/MTX in pharmaceutical field for cancer treatment   | 139  |
| Organo-clay (alkylammonium on MMT)             | methylene Blue (MB) (as a model drug)  | Intercalation process  | drug delivery system  | Thermo-sensitive hydrogel based on Pluronic and nanoclay potentially exploitable as injectable systems and as a long-term delivery system. | 141  |
| MMT clay                                       | tetracycline hydrochloride   | Ion exchange process   | antibacterial effect  | Gram-positive and Gram-negative bacteria   | 142  |
| MMT clay in polylactide matrix                 | gentamicin and neomycin  | Intercalation process  | antibacterial activity  | <i>Escherichia coli</i> ( <i>E. coli</i> )   | 143  |
| Smectite clays                                 | ciprofloxacin  | Ion exchange   | antibacterial Effect  | <i>E. coli</i> and <i>Staphylococcus aureus</i> ( <i>S. aureus</i> )   | 144  |
| MMT modified with PEGylated chitosan (PEG-CS)  | doxorubicin (DOX)  | Impregnation   | drug delivery   | TRAMP-C1 cells epithelial cell line  | 145  |
| Fe-MMT clay                                    | photosensitizer TPCI   | Ion exchange, intercalation  | photodynamic therapy, antibacterial effect, wound healing                             | <i>E. coli</i> , <i>Pseudomonas aeruginosa</i> ( <i>P. aeruginosa</i> ) and <i>S. aureus</i> In Vivo Antibacterial and Wound Healing Assay | 146  |
| HNTs   | vancomycin   | Physical dispersion, sonication, vacuuming   | local drug delivery system  | HL-60 cell lines (in vitro cell cytotoxicity) Antibacterial activity on <i>S. aureus</i> and <i>B. streptococcus</i>                       | 151  |
| HNTs   | ciprofloxacin and polymyxin B sulfate  | Physical dispersion, sonication, vacuuming   | wound dressing, antimicrobial activity  | <i>S. Aureus</i> and <i>P. aeruginosa</i>  | 153  |
| HNTs   | thymol   | Cryogel synthesis  | wound healing   | -  | 154  |
| HNTs   | DOX  | Impregnation   | drug delivery   | MFC mouse gastric cancer cells   | 156  |
| HNTs   | icariin  | Vacuum loading method  | bone tissue engineering   | In vitro osteogenic differentiation  | 161  |
| HNTs-Poly[bis(carboxyphenoxy)phosphazene]      | amoxicillin and marine sponge  | Inclusion and adsorption   | antibacterial and antibiofilm coating for the Ti-6Al-4V screw for dental implantation | <i>S. aureus</i> , <i>E. coli</i> , <i>Porphyromonas gingivalis</i>  | 164  |



Please do not adjust margins

|  |   |  |   | View Article Online<br>DOI: 10.1039/D4DT00757C  |
|--|---|--|---|---|
| HNTs   | deferoxamine  | Inclusion  | 3D-printed scaffold to realize the coupling regeneration of blood vessels and bones             | bone marrow mesenchymal stem cells (BMSCs), human umbilical endothelial cells (HUVECs)  |
| Saponites  | Gd-complexes  | Cation exchange  | diagnostic MRI and theranostics   | -   |
| Saponites  | Gd-(or Y <sup>3+</sup> )TETA-monoamide chelates         | Cation exchange  | diagnostic MRI and theranostics   | -   |
| Fe <sub>3</sub> O <sub>4</sub> @HNTs                                       | lanthanide complex, iron oxide                          | One-step hydrothermal process combined with the coupling grafting method | bioimaging and biological applications in human hepatic adenocarcinoma cells and diagnostic MRI | human hepatic (LO2) and human hepatic adenocarcinoma (HepG2) cell line, MRI was performed in vivo in tumor-bearing rabbits                        |
| Fe <sub>3</sub> O <sub>4</sub> – Laponite                                  | Fe <sub>3</sub> O <sub>4</sub>                          | Schikorr reaction  | localized magnetic hyperthermia (MH) and diagnostic MRI   | human glioblastoma cells (U87EGFRvIII) and human foreskin fibroblasts (HFF), MRI was performed in vivo in rodent brain                            |
| γ-ZP   | alendronate   | Exfoliation, topotactic exchange   | drug delivery capable of promoting bone mineralization and inhibiting bone resorption           | human bone osteosarcoma (MG-63)   |
| ZrP  | DOX   | Intercalation  | drug delivery of anticancer drugs   | MCF-7 and MDA-MB 231 cancer cell lines, MCF-10A cells, human prostate cancer PC3  |
| ZrP  | curcumin  | Adsorption   | drug delivery of anticancer drugs   | MDA-MB-231 breast cancer cell lines   |
| Fe <sub>3</sub> O <sub>4</sub> /α-ZrP                                      | 5-fluorouracil folate acid-chitosan-rhodamine6G complex | Exfoliation, intercalation   | deliver anticancer drug for tumor optical imaging and therapy                                   | A549, HeLa and HEK293 cells   |
| α-ZrP  | methylene blue  | Cation exchange  | photodynamic therapy  | MDA-MB-231 breast cancer cell   |
| α-ZrP/carboxymethyl cellulose  | chlorhexidine   | Intercalation, solvent casting   | antimicrobial and antibiofilm wound dressings   | HDF human dermal fibroblast cells (HuDe) and human keratinocyte (NCTC2544) cell lines   |
| α-ZrP  | Ag <sup>+</sup>   | Cation exchange  | antimicrobial   | <i>E. coli</i> Saos-2 (Sarcoma osteogenic) cell line  |
| α-ZrP/poly(lactide-co-glycolic acid)                                       | NorA efflux pump inhibitors                             | Intercalation, solvent casting   | antibiofilm composites  | <i>S. aureus</i> <i>Staphylococcus epidermidis</i>  |
| α-ZrP  | bromfenac   | Exfoliation, adsorption  | drug delivery of anti-inflammatory drug   | -   |
| α-ZrP  | caffeine  | Exfoliation, intercalation   | topical application   | -   |
| α-ZrP or LDH/poly(ethyleneoxideterephthalate)/poly(butylene terephthalate) | gentamicin, ciprofloxacin                               | Intercalation, melt-blending, melt extrusion                             | 3D scaffolds for bone infection prevention and tissue regeneration                              | <i>S. epidermidis</i> , <i>P. aeruginosa</i> cytotoxicity on human mesenchymal stromal cells (hMSCs) osteogenic differentiation capacity of hMSCs |
| Alg-Cu MOF-LDH beads   | DOX   | Co-precipitation and in-situ growth method.                              | drug delivery system for cancer therapy   | L929 non-cancerous cells, MCF-7 human breast cancer cells   |
| MgAl-LDH/poly(ε-caprolactone)  | LDH   | Electrospinning technique  | nanocomposite scaffolds   | mouse adipose derived stem cells (mADSC)  |
| graphene oxide   | graphene oxide nanosheets                               | Intercalation/exfoliation (Hummer's method)                              | antimicrobial surface coatings  | <i>E. coli</i>  |

#### 4.Applications of intercalation materials in polymer science

Clays and graphene have been extensively studied as filler of polymeric composite and the research has been summarised in





Please do not adjust margins

several reviews and thematic books. Therefore, to avoid being redundant, the main aspects related to polymeric composites based on these layered materials are entrusted to the most recent reviews and books.<sup>197-204</sup>

Here, the latest examples of the use of ZrP and LDHs as a filler of polymeric composites are reported. Table 4 summarises the recent applications of intercalation compounds based on ZrP and LDHs for polymer science.

#### 4.1 ZrP compounds for polymer science applications

Zirconium phosphate nanosheets, which size and thickness can be precisely controlled, are suitable nanofiller to improve the anti-corrosion properties of polymeric coatings.<sup>205</sup> It was shown, that mainly improved barrier properties, caused by self-assembly of ZrP nanosheets, are responsible for increased corrosion resistance of ZrP/epoxy resin (Fig. 10),<sup>206</sup> ZrP/polyurethane<sup>207</sup> or ZrP/polybenzoxazine coatings.<sup>208</sup>

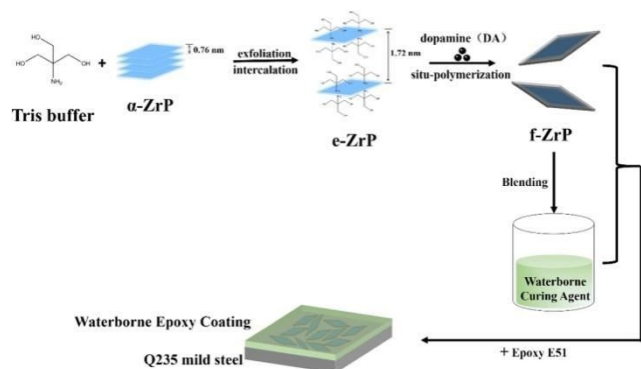


**Fig. 10** Exfoliation and functionalization process of  $\alpha$ -ZrP (f-ZrP) and the preparation of f-ZrP/WEP nanocomposite coatings. Reproduced with permission from ref. 206, Copyright 2020 Elsevier.

Zirconium phosphate is also a possible candidate for flame retardancy application due to its high thermal stability and phosphorus content. In addition, the aspect ratio and size of the nanoparticles can be controlled by the choice of synthesis and exfoliation method. Exfoliated ZrP significantly enhanced thermal stability and flame retardation behavior of polybenzoxazine by improving the stability of char layer and reducing the amount of flammable gases (Fig. 11).<sup>209</sup>

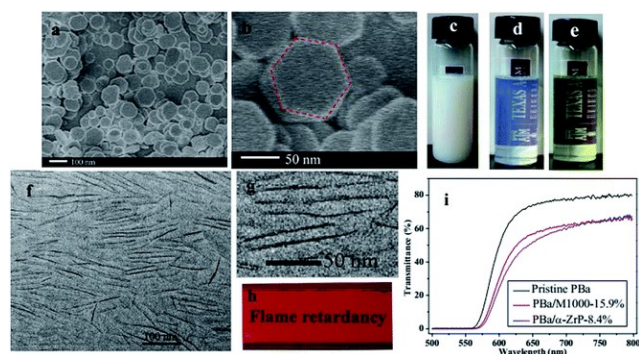


**Fig. 11** (a) and (b) SEM of original  $\alpha$ -ZrP, (c) original  $\alpha$ -ZrP in acetone, (d) exfoliated  $\alpha$ -ZrP in acetone, (e) Ba/ $\alpha$ -ZrP-8.4% in acetone, (f) and (g) TEM of PBa/ $\alpha$ -ZrP-8.4% nanocomposites, (h) photographic images of PBa/ $\alpha$ -ZrP-8.4% nanocomposites and (i) light transmission spectra of samples. Adapted with permission from ref. 209, Copyright 2016 Royal Society of Chemistry

Hybrid platelet nanostructure formed by self-assembly of ZrP, melamine and cyanuric acid significantly improved flame retardancy and crystallinity of polyamide6 (Fig. 12).<sup>210</sup> Acrylamide modified ZrP/polyacrylate nanocomposite was prepared via in situ polymerization and the effect of ZrP (dimension of ca. 120-160 nm) amount and quality of its dispersion on flame retardancy was described.<sup>211</sup> When ca. 0.5wt% of modified ZrP is added a decrease of nanoplatelets dimensions is visible because of the exfoliation process (Fig. 12 B-B'). The increase in ZrP content to 3 wt. % leads to the formation of big aggregates (Fig. 12 C-C') that might have a negative effect on the mechanical properties and flame retardancy of the composite.

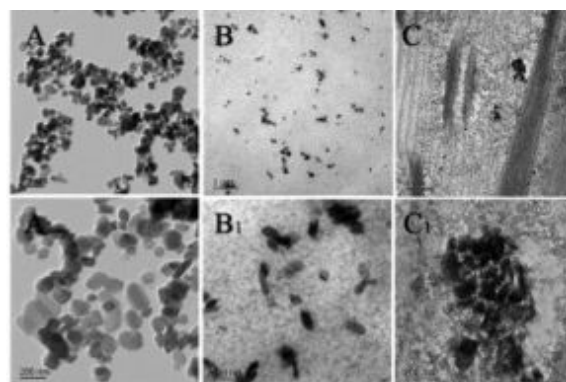


**Fig. 12** TEM images of ZrP/polyacrylate nanocomposite. A-A':  $\alpha$ -ZrP, B-B' and C-C': PPA/AM-ZrP-1 composites with 0.5 and 3wt%, respectively. Reproduced with permission from ref. 211, Copyright 2017 Royal Society of Chemistry.

ZrP nanoplates modified with hexachlorocyclotriphosphane and melamine in polyvinyl alcohol composite improve the yield and graphitization of char residues, make the char more stable, compact and continuous, inhibiting underlying polymer from contacting heat and oxygen.<sup>212</sup> The synergistic effect between polyphosphazene and  $\alpha$ -ZrP in polypropylene composites improved the thermal stability of the matrix and increased the amount of char yield in comparison with polypropylene containing either only polyphosphazene or only ZrP.<sup>213</sup> Organo-modified ZrP combined with other traditional flame retardant agent aluminium hydroxide leads to improving flame retardancy of ethylene vinyl acetate, low-density polyethylene/ethylene-vinyl acetate copolymer, and polystyrene.<sup>214,215</sup> Hierarchical graphene-confined zirconium phosphate nanosheets were used to improve thermal conductivity, mechanical properties and flame resistance of cellulose nanofiber aerogels.<sup>216</sup>



Please do not adjust margins

Using  $\alpha$ -ZrP nanosheets as nano-filler in polymers for food packaging application is very limited, some examples are given in Ghanbarzadeh's review.<sup>217</sup> Combination graphene and ZrP nanosheets with different two-dimensional scales results in a synergistic ordering effect that increased the tortuosity of permeation path for oxygen molecules to travel through the PVA nanocomposite films and significantly decreased their oxygen permeability. Similar nano-bricks wall architecture was obtained by layer-by-layer deposition of polyacrylic acid, poly (dimethyl diallyl ammonium chloride), and  $\alpha$ -ZrP nanosheets onto polyethylene terephthalate film (Fig. 13).<sup>218</sup> The oxygen transmission decreased exponentially with the number of the deposited quadlayers and the transparency of the film is not significantly reduced therefore this composite film shows great potential application in packaging.

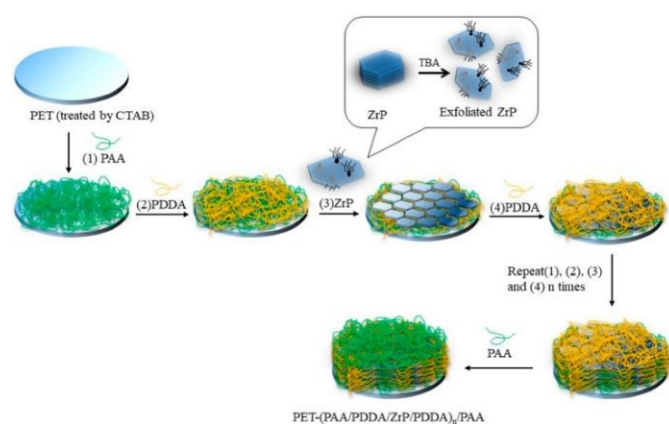


**Fig. 13** Schematic of the layer-by-layer (LbL) assembly for polyacrylic acid (PAA)/poly(dimethyl diallyl ammonium chloride) (PDPA)/zirconium phosphate (ZrP)/PDPA quadlayers. PET: polyethylene terephthalate; TBA: tetrabutylammonium; CTAB: hexadecyl trimethyl ammonium bromide. Reproduced with permission from ref. 218, Copyright 2018 MDPI.

#### 4.2 LDHs-based compounds for polymer science

LDHs are often used as polymer filler as they can be customised to accommodate functionalities such as fire retardancy, UV-stabilization, biocide, water or moisture permeability or repelling (increase of the hydrophobicity by the presence of platelets organo-modified by surfactants) while providing the expected barrier-effect by the enhancement of tortuosity coming from the high mechanical modulus of the anisotropic platelets<sup>219</sup>. More specifically, they may be of interest in food packaging by increasing the shelf life of food products and adding organoleptic and nutritional values.<sup>220</sup> LDH contribute to stabilizing or enhancing certain properties of PVC<sup>221</sup> or PBS.<sup>222</sup> In the latter case with organic anion interleaved into LDH fillers (L-tyrosine (TYR), L-tryptophan (TRP), L-ascorbate (ASA) and 3-

(4-hydroxyphenyl)propionate (HPP)), it was possible to exhibit antibacterial properties for the films in combination with a high chain extension effect suitable for polymer processability. When LDH intercalated with salicylate and rosmarinate anions are dispersed into LDPE, the formed polymer nanocomposites present strong antibacterial activity against *Staphylococcus aureus* and antioxidant properties altogether suitable for packaging materials.<sup>223</sup>

Furthermore, LDH has been used as a barrier to protect antioxidants from migrating out of the polymer.<sup>224</sup> Hindered phenolic antioxidants have gained widespread recognition and application in enhancing the heat resistance and oxidative aging performance of polypropylene (PP) composites.<sup>225</sup> However, the use of low molecular weight antioxidants poses certain challenges. These antioxidants have a greater tendency to volatilize, migrate, and be extracted from PP or PP-based products. Such behavior directly diminishes the anti-thermal oxidative aging efficacy of PP and its composites, and additionally presents a risk of contaminating food or drugs when used in packaging.<sup>226</sup> LDHs are highly desirable as antioxidant protection materials due to their adjustable compositions ( $M^{2+}$  and  $M^{3+}$ ) within the host sheet, replaceable interlayer anions ( $A^{n-}$ ) in the interlayer region, and adaptable charge density ( $M^{2+}/M^{3+}$  ratio). Consequently, it is plausible to inhibit the migration of antioxidants utilizing host-guest interactions and supramolecular forces by incorporating low molecular weight antioxidant species into the interlayer gaps of transparent LDHs. The 3-(3,5-di-tert-butyl-4-hydroxyphenyl)-propionate anions (AO, one-fourth of the most used antioxidant in industry, Irganox 1010) were intercalated into  $Mg_2Al$ -LDH, thus leading to AO-LDH samples by a one-step synthesis. Moreover, AO-LDH/PP composites were obtained through a solvent washing method. It was proven that the intercalation of AO anions between LDH led to an improvement of the antioxidative performance of PP composites. A barrier effect if offered by the host sheet of  $MgAl$ -AO-LDH thus allowing greater migration resistance than that of AO/PP composite.<sup>227</sup> Based on the theories, the composition of the host layer and the interlayer guests in the intercalation structure antioxidants were controlled to achieve the homogeneity of the additive compounding, leading to the construction of a class of supramolecular intercalated structure antioxidants with anti-migration, such as the single-intercalated  $MgAl$ -HALS-LDH photostabiliser.<sup>228</sup> and the co-intercalated  $CaAl$ -HxMy-LDH anti-aging agent.<sup>229</sup>

As far as corrosion inhibition is concerned, LDHs are found to be of interest also in polymer coatings for metal substrate such as magnesium alloys (AZ91D alloy of interest but lacking stability when exposed to marine environment) using the so-called self-healing behaviour of LDH cargo since the release is triggered by the corrosion.<sup>230</sup> LDHs can be mixed with other frameworks as exemplified in this article,<sup>231</sup> where the idea is to build a 3D fir tree-like hierarchical architecture by utilizing pulsed plasma electrolysis with LDHs and zeolitic imidazolate framework to protect magnesium alloy substrate.

**Table 4.** Most representative examples of intercalation compounds based on ZrP and LDHs in polymer science. The Reviews are not reported.



Please do not adjust margins

| Filler  | Polymeric matrix  | Preparation method                     | Purpose  | Performances  | Ref. |
|---|---|--|--|---|------|
| $\alpha$ -ZrP   | polydopamine (PDA)  | In-situ polymerization                 | Composite epoxy coating  | Corrosion protection (improved anticorrosion performance with $I_{\text{corr}}$ of $6.60 \times 10^{-9} \text{ A}\cdot\text{cm}^{-2}$ , which are one order of magnitude lower than that of blank epoxy coating)  | 206  |
| $\alpha$ -ZrP   | polyurethane  | In-situ polymerization                 | Advanced coatings  | Reduction of ca. 40% in $\text{H}_2\text{O}$ permeability, anti-corrosion protection  | 207  |
| $\alpha$ -ZrP   | polybenzoxazine   | thermal curing process                 | Flame retardance   | Improved thermal stability and flame retardancy (49.3% Peak of Heat Release Rate Reduction (PHRR) with respect to pure matrix)  | 209  |
| $\alpha$ -ZrP   | polyamide6  | melt blending                          | Flame retardance   | Improved flame retardancy (ca. 83% PHRR with respect to pure matrix)  | 210  |
| $\alpha$ -ZrP   | polyacrylate  | in-situ emulsion polymerization        | Flame retardance   | Improved flame retardancy. <i>LOI (Limited Oxygen Index) value of 25% against 23% of pure PPA</i>   | 211  |
| $\alpha$ -ZrP   | poly(vinyl alcohol)   | solution blending                      | Flame retardance   | Improved graphitization of char residues and thermal stability.   | 212  |
| $\alpha$ -ZrP   | Polypropylene   | melt blending                          | Flame retardance   | Improved formation of char residues and higher thermal stability with respect to pure matrix. <i>LOI value ca. 26% vs 17% in pure PP matrix</i>   | 213  |
| Organo-modified ZrP LDH (m-ZrP)   | ethylene vinyl acetate  | Melt blending                          | Flame retardance   | Incorporation of mZrP/LDH mixture into EVA/ATH composite resulted in a reduction in thermal stability but improved the char yield at 750 °C. EVA composites exhibited improvement in fire retardancy (decreased PHRR, THR, TSP and the enhanced char yield): LDH was more effective than mZrP in char formation; on the other hand, mZrP showed a 73 % reduction in PHRR, which was more efficient than LDH (58 % reduction in PHRR). | 214  |
| Organophilic $\alpha$ -ZrP  | low-density polyethylene and ethylene–vinyl acetate (LDPE/EVA) hybrid | Bradender extrusion                    | Flame retardance   | Improved flame retardancy. <i>LOI value of the composite ca. 32 against 20.3 of the pure polymer.</i>   | 215  |
| Hierarchical graphene-confined zirconium phosphate nanosheets (ZrP/RGO) | Cellulose-based aerogels  | unidirectional freeze-casing technique | Thermal insulation, Flame retardance, Mechanical properties                            | thermal conductivity ( $18 \text{ mW}\cdot\text{m}^{-1}\cdot\text{K}^{-1}$ ), and high LOI (33.5) as well as very low PHRR ( $14.1 \text{ kW/m}^2$ )  | 216  |
| $\alpha$ -ZrP   | PET film  | layer-by-layer (LbL) assembly          | Oxygen barrier properties  | oxygen transmission rate (OTR) reduced from 57 to $0.87 \text{ cc/m}^2/\text{day}$ for the best composite material.   | 218  |
| Organo-modified MgAl LDHs   | Polybutylene succinate (PBS)  | melt extrusion                         | viscoelastic properties, rate of hydrolysis, photo-degradation, antibacterial activity | small rate of hydrolysis, photo-stability, biocide activity, chain extension is obtained using a combination of LDHs-L-ascorbate and LDH-3-(4-hydroxyphenyl)propionate  | 222  |
| LDH-RA (RA=rosmarinic acid), LDH-SA (SA= salicylic acid)                | low-density polyethylene(LDPE)  | two-step melt compounding procedure    | antibacterial activity   | LDPE/MgAl-RA was selective and strongly inhibitory toward <i>S. aureus</i> , LDPE/ZnAl-SA inhibited the growth of <i>E. coli</i> and <i>S. aureus</i>   | 223  |
| LDH MgAl-D (D=3-(3,5-ditertbutyl-4-hydroxyphenyl)propionic acid)        | polypropylene   | solvent mixing method                  | anti-aging   | good stability against thermal aging, low migration of molecules out of the PP films  | 224  |
| LDH MgAl-AO (AO= Irganox 1010)  | polypropylene   | solvent mixing method                  | anti-aging   | LDH-AO significantly enhances long-term performance of LDH/PP composites against thermal/thermo-oxidative degradation   | 227  |
| LDH ZnAl-HxDy (H= 4-oxo-4-((2,2,6,6-tetramethylpiperidin-               | polypropylene   | solvent or extrusion mixing            | anti-aging   | the co-intercalated hybrid materials are found to decelerate the oxidative degradation for PP   | 228  |



Please do not adjust margins

|   |               |                        |            |   |  |
|---|---------------|------------------------|------------|---|--|
| 4-yl)amino)butanoic acid; D= 3-(3,5-ditertbutyl-4-hydroxyphenyl) propionic) |               |                        |            |   | View Article Online<br>DOI: 10.1039/D4DT00757C |
| LDH CaAl-HnMn'<br>(M= Irganox 1425; H= hindered amine light stabilizer)     | polypropylene | solvent casting method | anti-aging | Higher overall resistance against thermal degradation and photo-oxidation | 229  |

## Remarks and outlook

This perspective has focused on the role of intercalation chemistry as an evaluable tool for the design and synthesis of materials to meet some of the challenges of our century. Particular attention has been addressed to developing catalysts for producing clean energy, converting molecules derived from biomass into value-added products, degrading pollutants, materials for environmental remediation, systems for use in medicinal chemistry and for the preparation of polymeric composites.

As far as heterogeneous catalysts are concerned, the layered materials here reviewed provide sustainable catalyst sources with several advantages: easily recoverable and highly reusable, economical, efficient catalytic potential under mild conditions. The intercalation chemistry allows to obtain solids with transition metal species with large interest in the catalytic purposes. Metals can be intercalated as inorganic polycations within the interlayer space of clay (PILCs) or as cations or cationic complexes in ZrP. Transition metals can be inserted as constituents of the LDH layers. All these possibilities allowed to obtain catalysts with improvement of specific surface, thermal stability, dispersion of the active phase and sometimes catalytic performance thanks to specific interactions of the active species with the functional groups of the layer or their confinement in the interlayer region. Layered materials have been used as systems capable of favouring the growth of metallic nanoparticles upon intercalation of metallic ions followed by reduction in a confined environment. Otherwise, preformed metallic NPs can be immobilized on material surface. The confinement of NPs improves their resistance to cleavage and agglomeration as well as catalytic activity. In addition, the immobilization of the NPs favours their recovery and reuse. Recently, superior catalytic performance has been achieved by combining different materials to obtain heterostructures (*i.e.* TiO<sub>2</sub>/clays, HNT/MOFs, etc).

The ability of layered materials to intercalate ionic or molecular species has made them very good candidates as solid adsorbents for the removal of pollutants. The literature survey indicated that clays, ZrP and LDH can be successfully modified to improve the adsorption ability towards environmental contaminants thus making them potential candidate for wastewater treatments. The presence of intercalated functional groups (classically leading to an increase of the basal spacing, modification of textural properties and surface hydrophobicity) and, in some case, the increase in swelling ability are key factors affecting the adsorption properties of intercalated

compounds and leading to an improvement of adsorption properties with respect to raw materials.

ILCs can be also active as photocatalysts for pollutants degradation. This property is very often achieved in the case of compounds containing metal oxide particles, that can be thus stabilised from the layered matrices.

In this sense, efforts must be done in the searching of sustainable synthetic methods (especially in terms of time and production costs) for layered materials-based intercalation compounds. Few methods are for instance related to ultrasound accelerated synthesis. As a matter of example, environmentally safe low-cost adsorbents can indeed be obtained also starting from natural clays by using microwave-assisted heating methods.<sup>232</sup> Another emerging green and powerful synthesis is the mechanochemistry due its scalability and tunability. This technique has a high potential for the environmentally friendly production of layered materials for applications in the sustainable energy and environmental sectors.<sup>233</sup> Most of the papers in the recent literature are related to the use of ILCs for the removal of pollutants from simulated matrices. Since the solution pH, the presence of interfering ions and/or molecules can interfere on the main adsorption mechanism, the performances of materials must be tested in different conditions (*i.e.* distilled water, groundwater, industrial wastewater, sea water) to assess the real applicability of materials.<sup>234</sup>

Moreover, there are still problems to be solved in the use of materials as catalysts, especially when used to remove pollutants from water. For practical applications, a correct monitoring of the species formed during the catalytic reaction, together with the detection of possible toxic intermediates, have to be carried out.

For health purposes, the interlayer region of layered materials can be considered as a nanocontainer capable of protecting the bioactive species from light and oxygen. Moreover, the intercalation compounds, suitably modified, can act as target delivery of therapeutic species by releasing them upon a specific stimulus (variation of pH, temperature).

Among clays, halloysite is a promising local delivery system that does not require exfoliation or other complicated energy-consuming process, thus permitting the storage and controlled release of molecules.

The application of zirconium phosphate for drug delivery has not been extensively studied. However, the ability of ZrP to exfoliate in aqueous solution makes this material a good candidate to host bulky cations and basic species with therapeutic activity. Attention should be focused on scalable and green syntheses of ZrP, taking into account mechanochemistry. As for LDHs, the ILCs have long been



Please do not adjust margins

considered for the preparation of drug delivery systems. Future perspectives for these materials are related to the modulation of the layer composition, which can be constituted by several metal cations. The correct choice of these intralayer metals (i.e. Zn, Ga, Cu, Mg...), which can be released in appropriate media, can produce materials with therapeutic properties. In addition, a new frontier is the possibility of creating defect sites in the LDH layer that can be tailored to the needs of cancer immunotherapy. For photothermal/photodynamic therapy, sonodynamic therapy, and pH-sensitive magnetic resonance imaging, the modulation of defect sites in the crystal structure of LDH enables it to respond sensitively to external stimuli.<sup>235</sup>

Finally, layered materials have been used as nanofillers to improve the thermal stability, mechanical properties of polymers and anti-corrosion properties of polymeric coatings. The inorganic filler, intercalated with active species, absolves to another task that is to impart to the polymer additional properties such as antioxidant and antimicrobial properties.

However, in general, one of the major issues in materials development in many areas is scaling up from the laboratory level to large-scale implementation as an available and affordable commercial solution. The production of large quantities of intercalation compounds means simplification of preparation steps, elimination of toxic solvents/reagents, and reduced production costs. The latter could be overcome by using waste materials where possible, in accordance with the principles of the circular economy.

The recovery and reuse processes of these adsorbents are not always studied in the literature. Moreover, the fate of recovered pollutants merits additional consideration to develop sustainable and circular economy processes.<sup>234</sup> An interesting example of Cr-based PILCs for the recovery of anionic and cationic, especially focusing on the possibility of reducing the synthesis time and cost and to identify the optimal conditions for effective adsorption of individual dyes using Cr pillared clay after statistical analysis through the design of experiments was recently reported in the literature.<sup>236</sup> Moreover, in many cases, we must continue efforts to understand the structure-property relationship. As an example, for PILCs different characterisation techniques are needed to reveal the still unknown properties of PILCs thus paving the way for intelligent material design.

## Conflicts of interest

There are no conflicts to declare.

## Acknowledgements

All co-authors as well as all colleagues from the board of the International Symposium on Intercalation Compounds (ISIC) are warmly acknowledged.

## Notes and references

View Article Online

DOI: 10.1039/D4DT00757C

- 1 M. Massaro, R. Noto and S. Riela, *Molecules*, 2020, **25**, 4863.
- 2 S. Nawaz, M. Ahmad, S. Asif, J. J. Klemes, M. Mubashir, M. Munir, M. Zafar, A. Bokhari, A. Mukhtar, S. Saqib, K. S. Khoo and P. L. Show, *Bioresour. Technol.* 2022, **343**, 126068.
- 3 A. Ramli, M. Farooq, A. Naeem, S. Khan, M. Hummayun, A. Iqbal, S. Ahmed and L.A. Shah, in *Frontiers in Bioenergy and Biofuels*, eds. E. Jacob-Lopes and L. Queiroz Zepka, *IntechOpen*, 2017, **14**, 285–308.
- 4 T. Chellapandi and G. Madhumitha, *Mol. Divers.*, 2022, **26**, 2311–2339.
- 5 S. Sadjadi, *Applied Clay Sci.*, 2020, **189**, 105537.
- 6 Y. Li, X. Yuan, L. Jiang, H. Dai, Y. Zhao, X. Guan, J. Bai and H. Wang, *Environ. Sci.: Nano*, 2022, **9**, 841–866.
- 7 Y. Zheng, L. Wang, F. Zhong, G. Cai, Y. Xiao and L. Jiang, *Ind. Eng. Chem. Res.*, 2020, **59**, 5636–5647.
- 8 Y. H. Ahmad, A. T. Mohamed and S. Y. Al-Qaradawi, *Appl. Clay Sci.*, 2021, **201**, 105956.
- 9 N. M. Sanchez-Ballester, G. V. Ramesh, T. Tanabe, E. Koudelkova, J. Liu, L. K. Shrestha, Y. Lvov, J. P. Hill, K. Ariga and H. Abe, *J. Mater. Chem. A*, 2015, **3**, 6614–6619.
- 10 F. Carniato, C. Bisio, R. Psaro, L. Marchese and M. Guidotti, *Angew. Chem. Int. Ed.* 2014, **53**, 10095–10098.
- 11 F. Carniato, C. Bisio Chiara, C. Evangelisti, R. Psaro, L. Marchese and M. Guidotti, *Dalton Trans.*, 2018, **47**, 2939–2948.
- 12 S. Marchesi, M. Guidotti, L. Marchese, F. Carniato and C. Bisio, *Chem. Eur. J.* 2021, **27** (14), 4723–4730.
- 13 E. M. Serwicka, *Catalysts*, 2021, **11**, 1087.
- 14 K. Bahranowski, W. Włodarczyk, E. Wisła-Walsh, A. Gawel, J. Matusik, A. Klimek, B. Gil, A. Michalik-Zym, R. Dula and R.P. Socha, *Microp. Mesop. Mater.*, 2015, **202**, 155–164.
- 15 B. Szczepanik, *Appl. Clay Sci.*, 2017, **141**, 227–239.
- 16 M. Kashif, M. Yuan, Y. Su, P.M. Heynderickx and A. Memon, *Appl. Clay Sci.*, 2023, **233**, 106847.
- 17 M. C. Dlamini, M. S. Maubane-Nkadimeng and J. A. Moma, *J. Environ. Chem. Eng.*, 2021, **9**, 106546.
- 18 S. Yoda, Y. Sakurai, A. Endo and T. Miyata, *J. Mater. Chem.*, 2004, **14**, 2763–2767.
- 19 D. Chen, Q. Zhu, F. Zhou, X. Deng and F. Li, *J. Hazard. Mater.*, 2012, **235–236**, 186–193.
- 20 L. Chmielarza, A. Kowalczyk, M. Skoczek, M. Rutkowska, B. Gil, P. Natkański, M. Radko, M. Motak, R. Dębek and J. Ryczkowski, *Appl. Clay Sci.*, 2018, **160**, 116–125.
- 21 M. Pica, *Catalysts*, 2017, **7**, 190.
- 22 H. Ding, A. Ahmed, K. Shen and L. Sun, *Aggregate*, 2022, **3**, e174.
- 23 F. Wang, Z. Yuan, B. Liu, S. Chen and Z. Zhang, *J. Ind. Eng. Chem.*, 2016, **38**, 181–185.
- 24 C. Zhu, Q. Liu, D. Li, H. Wang, C. Zhang, C. Cui, L. Chen, C. Cai and L. Ma, *ACS Omega*, 2018, **3**, 7407–7417.
- 25 M. Chen, J. Xia, H. Li, X. Zhao, Q. Peng, J. Wang, H. Gong, S. Dai, P. An, H. Wang and Z. Hou, *ChemCatChem*, 2021, **13**, 3801–3814.
- 26 J. He, Y. Jiang, B. Ding, Y. Wang, H. Qiu, S. Dai, X. Zhao and Z. Hou, *Appl. Catal. A-Gen.*, 2023, **664**, 119351.



Please do not adjust margins

- 27 M. Pica, M. Nocchetti, B. Ridolfi, A. Donnadio, F. Costantino, P. L. Gentili and M. Casciola, *J. Mater. Chem. A*, 2015, **3**, 5525–5534.
- 28 M. Pica, S. Calzuola, A. Donnadio, P. L. Gentili, M. Nocchetti and M. Casciola, *Catalysts*, 2019, **9**, 3.
- 29 Y. Xu, F. Zhou, M. Chen, H. Hu, L. Lin, J. Wua and M. Zhanga, *New J. Chem.*, 2020, **44**, 9793–9801.
- 30 L. Lin, Y. Wen, Li, Y. Tan, P. Yang, Y. Liang, Y. Xu, H. Hu and Y. Xu, *Nanomaterials*, 2022, **12**, 3339.
- 31 J. Zhou, H. Sun, C. Xu, Z. Wang, H. Zhang, D. Guo, J. Zhang, X. Ji, L. Liu, J. Ma and Z. Tong, *J. Taiwan Inst. Chem. Eng.*, 2022, **138**, 104478.
- 32 M. V. Ramos-Garcés and J. L. Colón, *Nanomaterials*, 2020, **10**, 822.
- 33 M.V. Ramos-Garcés, J. Sanchez, D.E. Del Toro-Pedrosa, I.B. Alvarez, Y. Wu, E. Valle, D. Villagrán, T.F. Jaramillo and J.L. Colón, *ACS Appl. Energy Mater.*, 2019, **2**, 3561–3567.
- 34 M. V. Ramos-Garcés, J. Sanchez, K. La Luz-Rivera, D. E. Del Toro-Pedrosa, T. F. Jaramillo and J. L. Colón, *Dalton Trans.*, 2020, **49**, 3892–3900.
- 35 J. Sanchez, M. Burke Stevens, A. R. Young, A. Gallo, M. Zhao, Y. Liu, M. V. Ramos-Garcés, M. Ben-Naim, J. L. Colón, R. Sinclair, L. A. King, M. Bajdich and T. F. Jaramillo, *Adv. Energy Mater.*, 2021, **11**, 2003545.
- 36 S. Kumar, A. Yoyakki, A. Pandikassala, R. Soni and S. Kurungot, *Adv. Sustainable Syst.*, 2023, **7**, 2200330.
- 37 A. Sharma, S. Kumari, S. Sharma, T. Singh, S. Kumar, A. Thakur, S. K. Bhatia and A. K. Sharma, *Mater. Today Sustain.*, 2023, **22**, 100399.
- 38 J.Wu, Y. Xie, Y. Li, M. Jin, L. Liu, G. Pan, C.Wang and F. Li, *Coord. Chem. Rev.*, 2023, **497**, 215437.
- 39 B. Sardar and D. Srimani, *Tetrahedron*, 2023, **138**, 133414.
- 40 Y. Xiao, J. Li, Y. Tan, X. Chen, F. Bai, W. Luo and Y. Ding, *Int. J. Mol. Sci.*, 2023, **24** (19), 14859.
- 41 C. Gastaldi, C. Taviot-Gueho, C. Guerard-Helaine and C. Forano, *Appl. Clay Sci.*, 2023, **238**, 106931.
- 42 L. Izquierdo-Aranda, R. Adam and J. R. Cabrero-Antonino, *ChemSusChem.*, 2023, **16**, e2023008.
- 43 U. A. Mohanty, D. P. Sahoo, L. Paramanik and K. Parida, *Sustainable Energy Fuels*, 2023, **7**, 1145–1186.
- 44 Y. Liu, Y. Guo, Y. Liu, Z. Wei, K. Wang and Z. Shi, *Energy Fuels*, 2023, **37**, 2608–2630.
- 45 P. R. Chowdhury, H. Medhi, K. G. Bhattacharyya and C. M. Hussain, *Coord. Chem. Rev.*, 2024, **501**, 215547.
- 46 D. K. Perivoliotis, J. Ekspong, X. Zhao, G. Hu, T. Wagberg and E. Gracia-Espino, *Nano Today*, 2023, **50**, 101883.
- 47 Y. Liao, R. He, W. Pan, Y. Li, Y. Wang, J. Li and Y. Li, *Chem. Eng. J.*, 2023, **464**, 142669.
- 48 Z.-Q. Liu, X. Liang, F.-X. Ma, Y.-X. Xiong, G. Zhang, G. Chen, L. Zhen, C.-Y. Xu, *Adv. Energy Mater.*, 2023, **13**, 2203609.
- 49 R. Dai, C. Dai, S. Hou, Q. He, B. Liu, M. Huang, H. Jiang, M. Li, L. Pan and Z. Guo, *J. Mater. Chem. A.*, 2023, **11**, 20383–20407.
- 50 D.Tyndall, M. J. Craig, L. Gannon, C. McGuinness, N. McEvoy, A. Roy, M. Garcia-Melchor, M. P. Browne and V. Nicolosi, *J. Mater. Chem. A.*, 2023, **11**, 4067–4077.
- 51 A. Zitolo, V. Goellner, V. Armel, M.-T. Sougrati, T. Mineva, I. Stievano, E. Fonda and F. Jaouen, *Nat. Mater.*, 2015, **14**, 937–942.
- 52 J. Duan, S. Chen, M. Jaroniec and S. Z. Qiao, *ACS Catal.*, 2015, **5**, 5207–5234.
- 53 M. K. Uddin, *Chem. Eng. J.*, 2017, **308**, 438–462.
- 54 V. B. Yadav, R. Gadi and S. Kalr, *J. Environ. Manage.*, 2019, **232**, 803–817.
- 55 S. Manna, P. Das, P. Basak, A. K. Sharma, V. K. Singh, R. K. Patel, J. K. Pandey, V. Ashokkumar and A. Pugazhendhi, *Chemosphere*, 2021, **280**, 130961.
- 56 S. Marchesi, F. Carniato, M. Guidotti, M. Botta, L. Marchese and C. Bisio, *New Journal of Chemistry*, 2020, **44**, 10033–10041.
- 57 S. Marchesi, S. Nascimbene, M. Guidotti, C. Bisio and F. Carniato, *Dalton Trans.*, 2022, **51**, 4502–4509.
- 58 S. Marchesi, C. Bisio and F. Carniato, *RSC Adv.*, 2020, **10**, 29765–29771.
- 59 T. Zhang, W. Wang, Y. Zhao, H. Bai, T. Wen, S. Kang, G. Song, S. Song and S. Komarneni, *Chem. Eng. J.*, 2021, **420**, 127574.
- 60 H. Bai, Y. Zhao, X. Zhang, W. Wang, T. Zhang, C. Liu, H. Yi and S. Song, *J. Am. Ceram. Soc.*, 2019, 3908–3922.
- 61 H. Bai, Y. Zhao, W. Wang, T. Zhang, H. Yi and S. Song, *Ceram. Int.*, 2019, **45**, 17054–17063.
- 62 D.A. Almasri, N.B. Saleh, M.A. Atieh, G. McKay and S. Ahzi, *Sci. Rep.*, 2019, **9**, 1–13.
- 63 D. Yao, Y. Shi, H. Pan, D. Zhong, H. Hou, X. Wu, J. Chen, L. Wang, Y. Hu and J.C. Crittenden, *Chem. Eng. J.*, 2020, **392**, 123637.
- 64 X. Zhang, S. Lin, X.Q. Lu and Z.L. Chen, *Chem. Eng. J.*, 2010, **163**, 243–248.
- 65 Y. Zhang, Y. Li, J. Li, L. Hu and X. Zheng, *Chem. Eng. J.*, 2011, **171**, 526–531.
- 66 N. Arancibia-Miranda, S.E. Baltazar, A. García, D. Munoz-Lira, P. Sepúlveda, M. A. Rubio and D. Altbir, *J. Hazard. Mater.*, 2016, **301**, 371–380.
- 67 N. Ezzatahmedi, G. A. Ayoko, G. J. Millar, R. Speight, C. Yan, J. Li, S. Li, J. Zhu and Y. Xi, *Chem. Eng. J.*, 2017, **312**, 336–350.
- 68 M.R. Olson, T.C. Sale, C.D. Shackelford, C. Bozzini and J. Skeean, *Ground Water Monit. Rem.*, 2012, **32**, 63–74.
- 69 A. M. Awad, S. M. R. Shaikh, R. Jalab, M. H. Gulied, M. S. Nasser, A. Benamor and S. Adham, *Sep. Purif. Technol.*, 2019, **228**, 115719.
- 70 Y. Park, G.A. Ayoko and R.L. Frost, *J. Colloid Interface Sci.*, 2011, **354**, 292–305.
- 71 Q. Yang, M. Gao, Z. Luo and S. Yang, *Chem. Eng. J.*, 2016, **285**, 27–38.
- 72 G. Xue, M. Gao, Z. Gu, Z. Luo and Z. Hu, *Chem. Eng. J.*, 2013, **218**, 223–231.
- 73 A. Abutaleb, M. Imran, N. Zouli, A. H. Khan, S. Hussain, M.A. Ali, O.Bakather, M. A. Gondal, N. A. Khan, H. Panchal and S. Zahmatkesh, *Chemosphere*, 2023, **316**, 137824.
- 74 C.V. Lazaratou, D.V. Vayenas and D. Papoulis, *Appl. Clay Sci.*, 2020, **185**, 105377.
- 75 A. Kausar, M. Iqbal, A. Javed, K. Aftab, Z. Nazli, H. N. Bhatti and S. Nouren, *J. Mol. Liq.*, 2018, **256**, 395–407.



Please do not adjust margins

- 76 M. A. Moreira, K. J. Ciuffi, V. Rives, M. A. Vicente, R. Trujillano, A. Gil, S. A. Korili and E. H. de Faria, *Appl. Clay Sci.*, 2017, **135**, 394–404.
- 77 T. Ngulube, J. R. Gumbo, V. Masindi and A. Maity, *J. Environ. Manage.*, 2017, **191**, 35–57.
- 78 H. Han, M. K. Rafiq, T. Zhou, R. Xu, O. Mašek and X. Li, *J. Hazard. Mater.*, 2019, **369**, 780–796.
- 79 N. Belhouchat, H. Zaghoulane-Boudiaf and C. Viseras, *Appl. Clay Sci.*, 2017, **135**, 9–15.
- 80 H. Zaghoulane-Boudiaf, M. Boutahala, S. Sahnoun, C. Tiar and F. Gomri, *Appl. Clay Sci.*, 2014, **90**, 81–87.
- 81 Q. Cui and B. Chen, *Appl. Clay Sci.*, 2023, **235**, 106869.
- 82 M. Arif, G. Liu, B. Yousaf, R. Ahmed, S. Irshad, A. Ashraf, M. Ziaur-Rehman and M. S. Rashid, *J. Cleaner Prod.*, 2021, **310**, 127548.
- 83 M. M. Mian and G. Liu, *Chem. Eng. J.*, 2020, **392**, 123681.
- 84 K.S.D.Premarathna, A. Upamali, B. Sarkar and E. E. Kwon, *Chem. Eng. J.*, 2019, **372**, 536–550.
- 85 P. Pandey and V. K. Saini, *Environ. Chem. Lett.*, 2019, **17**, 721–727.
- 86 Z. Huang, P. Wu, B. Gong, Y. Dai, P. C. Chiang, X. Lai and G. Yu, *PLoS ONE*, 2016, **11**, e0159802.
- 87 M. Ding, S. Zuo and C. Qi, *Appl. Clay Sci.*, 2015, **115**, 9–16.
- 88 C. Liu, Z. Li, B. Li, H. Zhang and J. Han, *Appl. Clay Sci.*, 2023, **236**, 106887.
- 89 A. Bashir, S. Ahad, L. A. Malik, A. Qureshi, T. Manzoor, G. N. Dar and A. H. Pandith, *Ind. Eng. Chem. Res.*, 2020, **59**, 22353–22397.
- 90 M. Pica, *Molecules*, 2021, **26**, 2392.
- 91 R. Chakraborty, K. Bhattacharaya and P. Chattopadhyay, *Appl. Radiat. Isot.*, 2014, **85**, 34–38.
- 92 W. J. Mu, Q. H. Yu, R. Zhang, X. L. Li, R. Hu, Y. He, H. Y. Wei, Y. Jian and Y. C. Yang, *J. Mater. Chem. A*, 2017, **5**, 24388–24395.
- 93 A. Bashir, L. A. Malik, G. N. Dar and A. H. Pandith, in *Application of Ion Exchange Materials in the Environment*, eds. A. M. Inamuddin and A. Assiri, Springer, Cham, 2019, 95–108.
- 94 W. J. Mu, S. Z. Du, Q. H. Yu, X. L. Li, H. Y. Wei, Y. C. Yang and S. M. Peng, *Chem. Eng. J.*, 2019, **361**, 538–546.
- 95 T. Takei, K. Iizuka, A. Miura, S. Yanagida, N. Kumada, E. Magome, C. Moriyoshi and Y. Kuroiwa, *Langmuir*, 2016, **32**, 9993–9999.
- 96 Y. Cheng, X. D. Wang, S. Jaenicke and G. K. Chuah, *Inorg. Chem.*, 2018, **57**, 4370–4378.
- 97 S. Bevara, P. Giri, S. J. Patwe, S. N. Achary, R. K. Mishra, A. Kumar, A. K. Sinha, C. P. Kaushik and A. K. Tyagi, *J. Environ. Chem. Eng.*, 2018, **6**, 2248–2261.
- 98 Y. Cheng, S. S. Y. Chui, X. D. T. Wang, S. Jaenicke and G. K. Chuah, *Inorg. Chem.*, 2019, **58**, 13020–13029.
- 99 Y. Cheng, H. W. Zhang, J. A. Jaenicke, E. C. P. Tan and G. K. Chuah, *ACS Sustain. Chem. Eng.*, 2019, **7**, 895–904.
- 100 W. J. Mu, Q. H. Yu, J. Y. Gu, X. L. Li, Y. C. Yang, H. Y. Wei and S. M. Peng, *Sep. Purif. Technol.*, 2020, **240**, 116658.
- 101 A. M. Bakry, F. S. Awad, J. A. Bobb, A. A. Ibrahim and M. S. El-Shall, *RSC Adv.*, 2020, **10**, 37883–37897.
- 102 S. Fujimoto, T. Takei, S. Yanagida and N. Kumada, *J. Ceram. Soc. Jpn.*, 2019, **127**, 830–836.
- 103 R. Silbernagel, C. H. Martin, A. Clearfield, *Inorg. Chem.*, 2016, **55**, 1651–1656. DOI: 10.1039/D4DT00757C
- 104 M. W. Terban, C. Shi, R. Silbernagel, A. Clearfield and S. J. L. Billinge, *Inorg. Chem.*, 2017, **56**, 8837–8846.
- 105 S. Pourbeyram, *Ind. Eng. Chem. Res.*, 2016, **55**, 5608–5617.
- 106 T. Ahamad, M. Naushad, B. M. Al-Maswari, J. Ahmed, Z. A. Allothman, S. M. Alshehri and A. A. Alqadami, *J. Ind. Eng. Chem.*, 2017, **53**, 268–275.
- 107 X. L. Zhang, J. L. Shen, S. Y. Pan, J. S. Qian and B. C. Pan, *Adv. Funct. Mater.*, 2020, **30**, 1909014.
- 108 D. D. Zhao, Y. Yu and J. P. Chen, *Water Research*, 2016, **101**, 564–573.
- 109 J. H. Xu, R. Koivula, W. Z. Zhang, E. Viikinkoski, S. Hietala and R. Harjula, *Hydrometallurgy*, 2018, **175**, 170–178.
- 110 Y. Ibrahim, E. Abdulkarem, V. Naddeo, F. Banat and S. W. Hasan, *Sci. Total Environ.*, 2019, **690**, 167–180.
- 111 R. Bhatt, V. Ageetha, S. B. Rathod and P. Padmaja, *Carbohydr. Polym.*, 2019, **208**, 441–450.
- 112 M. Thakur, D. Pathania, G. Sharma, M. Naushad, A. Bhatnagar and M. R. Khan, *J. Polym. Environ.*, 2018, **26**, 1415–1424.
- 113 Y. Zhu, T. Shimizu, T. Kitajima, K. Morisato, N. Moitra, N. Brun, T. Kiyomura, K. Kanamori, K. Takeda, H. Kurata, M. Tafu and K. Nakanishi, *New J. Chem.*, 2015, **39**, 2444–2450.
- 114 Q. R. Zhang, Y. X. Li, P. Phanlavong, Z. K. Wang, T. F. Jiao, H. Qiu and Q. M. Peng, *J. Clean Prod.*, 2017, **161**, 317–326.
- 115 S. Qing, H. Chen, L. J. Han, Z. B. Ye, L. T. Shi, Z. Shu, L. Chen, L. Xu and Q. Q. Xu, *ACS Omega*, 2020, **5**, 27873–27879.
- 116 Y. J. Zhou, J. J. Liu, M. Xiao, Y. Z. Meng and L. Y. Sun, *ACS Appl. Mater. Interfaces*, 2016, **8**, 5547–5555.
- 117 L. Ma, Q. Wang, S. M. Islam, Y. Liu, S. Ma. and M.G. Kanatzidis, *J. Am. Chem. Soc.*, 2016, **138** (8), 2858–2866.
- 118 D. Cosano, D. Esquivel, F. J. Romero-Salguero, C. Jimenez-Sanchidrian, J. Rafael Ruiz, *Langmuir*, 2023, **39**, 5294–5305.
- 119 A. Haleem, A. Shafiq, S.-Q. Chen and M. Nazar, *Molecules*, 2023, **28**, 1081.
- 120 Y.-D. Dong, Y. Shi, Y.-L. He, S.-R. Yang, S.-Y. Yu, Z. Xiong, H. Zhang, G. Yao, C.-S. He and B. Lai, *Ind. Eng. Chem. Res.*, 2023, **62**, 10828–10848.
- 121 Z. Bi, R.-T. Guo, X. Hu, J. Wang, X. Chen, and W.-G. Pan, *Nanoscale*, 2022, **14** (9) 3367–3386.
- 122 C. Zhao, L. Wang, L. Huang, N. M. Musyoka, T. Xue, J. Rabeah and Q. Wang, *J. Energy Chem.*, 2024, **90**, 435–452.
- 123 Z.-Y. Zhang, H. Tian, L. Bian, S.-Z. Liu, Y. Liu, Z.-L. Wang, *J. Energy Chem.*, 2023, **83**, 90–97.
- 124 X. Xu, J. Wang, A. Zhou, S. Dong, K. Shi, B. Li, J. Han, and D. O'Hare, *Nat. Commun*, 2021, **12**, 3069.
- 125 P. Zhang, J. Li, L. Lv, Y. Zhao and L. Qu, Liangti, *ACS Nano*, 2017, **11**, 5087–5093.
- 126 J. Xue, S. Ma, Y. Zhou, Z. Zhang and M. He, *ACS Appl. Mater. Interfaces*, 2015, **7**(18), 9630–9637.
- 127 G. Mishra, B. Dash, and S. Pandey, *Appl. Clay Sci.*, 2018, **153**, 172–186.
- 128 T. Hu, X. Mei, Y. Wang, X. Weng, R. Liang and M. Wei, *Sci. Bull.*, 2019, **64**, 1707–1727.



Please do not adjust margins

- 129 Figueiredo Gomes, J. Hamilton Gomes and E. Ferreira da Silva, *Environ. Geochem. Health*, 2020, **42**, 3507–3527.
- 130 P. Das, S. Manna, A. K. Behera, M. Shee, P. Basak and A. K. Sharma, *Environ. Res.*, 2022, **212**, 113534–123546.
- 131 A. Sharma, G. R. Kokil, Y. He, B. Lowe, A. Salam, T. A. Altalhi, Q. Ye and T. Kumeria, *Bioact. Mater.*, 2023, **24**, 535–550.
- 132 C. de Sousa Figueiredo Gomes, *Environ. Geochem. Health*, 2018, **40**, 1739–1765.
- 133 N. Khatoun, M. Q. Chu and C. H. Zhou, *Mater. Chem. B*, 2020, **8**, 7335–7351.
- 134 L. Jia, T. Zhou, J. Xu, Z. Xu, M. Zhang, Y. Wang, Z. Li, and T. Zhu, *J. Mater. Sci.*, 2016, **5**, 1324–1332.
- 135 S. Murugesan and T. Scheibel, *J. Polym. Sci.*, 2021, **59**, 1610–1642.
- 136 H. Tomás, C. S. Alves and J. Rodrigues, *Nanomedicine: NBM*, 2018, **14**, 2407–2420.
- 137 Y. M. Lvov, Y. M. M. DeVilliers and R. F. Fakhrullin, *Expert Opin. Drug Deliv.* 2016, **13**, 977–986.
- 138 H. Y. Kim, J. H. Jae, H. Cheon, S. H. Lee, J. Y. Min, S.-Y. Back, J. G. Song, D. H. Kim, J.-J. Lim and H.-K. Han, *J. Nanobiotechnology*, 2020, **18**, 17–31.
- 139 A. I. Voicu, S. A. Gârea, A. Ghebaur, C. L. Nistor, A. Sârbu, E. Vasile, R. Mitran and H. Iovu, *Microp. Mesop. Mater.*, 2021, **328**, 111434.
- 140 F. García-Villén and C. Viseras, *Pharmaceutics*, 2020, **12**, 1142–1150.
- 141 C. Tipa, M. T. Cidade, T. Vieira, J. C. Silva, P. I. P. Soares and J. P. Borges, *Nanomater.*, 2021, **11** (1), 25–47.
- 142 K. Dutta, K. Saha, P. Sarkar and D. Chattopadhyay, *Bull. Mater. Sci.*, 2020, **43**(1) 248–257.
- 143 A. Rapacz-Kmita, B. Szaraniec, M. Mikołajczyk, E. Stodolak-Zych, E. Dzierzkowska, M. Gajek and P. Dudek, *Acta Bioeng. Biomech.*, 2020, **22** (2) 83–93.
- 144 C. F. Memenfo, N. Tabary, J. A. Mbey, S. Degoutin, F. Cazaux, M. Bacquet, M. Maton, B. Martel and D. Njopwouo, *J. Mater. Sci. Chem. Eng.*, 2021, **9**, 21–40.
- 145 H.-J. Huang, S.-Y. Huang, T.-H. Wang, T.-Y. Lin, N.-C. Huang, O. Shih, U.-S. Jeng, C.-Y. Chu and W.-H. Chiang, *Carbohydr. Polym.*, 2023, **302**, 120390.
- 146 J. J. Zhang, F. Zhou, Z. He, Y. Pan, S. Zhou, C. Yan, L. Luo and Y. Gao, *ACS App. Mater. & Inter.*, 2022, **14** (27), 30533–30545.
- 147 D. Peixoto, I. Pereira, M. Pereira-Silva, F. Veiga, M. R. Hamblin, Y. Lvov, M. Liu and A. C. Paiva-Santos, *Coord. Chem. Rev.*, 2021, **440**, 213956.
- 148 M. Massaro, C. G. Colletti, G. Lazzara and S. Riela, *J. Funct. Biomater.*, 2018, **9**, 58–70.
- 149 D. Sawicka, L. Zapor, L. Chojnacka-Puchta and K. Miranowicz-Dzierzawska, *Toxicol Res.*, 2021, **37**, 301–31.
- 150 G. Biddeci, G. Spinelli, P. Colomba and F. Di Blasi, *Int. J. Mol. Sci.*, 2023, **24**(5), 4801–4822.
- 151 Q. Pan, N. Li, Y. Hong, H. Tang, Z. Zheng, S. Weng, Y. Zheng and L. Huang, *RSC Adv.*, 2017, **7** (34), 21352–21359.
- 152 M. Barman, S. Mahmood, R. Augustine, A. Hasan, S. Thomas and K. Ghosal, *Intern. J. Biol. Macrom.*, 2020, **162**, 1849–1861.
- 153 R. Shi, Y. Niu, M. Gong, J. Ye, W. Tian and L. Zhang, *Mater. Sci. Eng. C*, 2018, **87**, 128–138. DOI: 10.1039/D4DT00757C
- 154 C. Zagni, A. A. Scamporrino, P. M. Riccobene, G. Floresta, V. Patamia, A. Rescifina and S. C. Carroccio, *Nanomaterials*, 2023, **13**, 741.
- 155 R. Arshad, M. S. Arshad, A. Rahdar, D. Hassan, R. Behzadmehr, S. Ghotekar, D. I. Medina and S. Pandey, *J. Drug. Deliv. Sci. Technol.*, 2023, **83**, 104432–104444.
- 156 K. Li, Y. Zhang, M. Chen, Y. Hu, W. Jiang, L. Zhou, S. Li, M. Xu, M., Q. Zhao, and R. Wan, *Int. J. Nanomed.*, 2018, **13**, 19–30.
- 157 M. Perveen, S. Nazir, A. W. Arshad, M. I. Khan, M. Shamim, K. Ayub, M. A. Khan and J. Iqbal, *Biophys. Chem.*, 2020, **267**, 106461–106473.
- 158 E. Naumenko and R. Fakhrullin, *Biotechnol. J.*, 2019, e1900055.
- 159 E. Gkouma, E. Gianni, K. Avgoustaki and D. Papoulis, *App. Clay Sci.*, 2021, **214**, 106291.
- 160 L. W. Wong, C. B. S. Goh, P. Pasbakhsh and J. B. L. Tan, *J. Sci-Adv. Mater. Dev.*, 2022, **7**, 100431–100445.
- 161 F. Kazemi-Aghdam, V. Jahed, M. Dehghan-Niri, F. Ganji and E. Vasheghani-Farahani, *Carbohydr. Polym.*, 2021, **269**, 118311–118320.
- 162 M. A. Bonifacio, A. Cochis, S. Cometa, A. Scalzone, P. Gentile, G. Procino, S. Milano, A. C. Scalia, L. Rimondini and E. De Giglio, *Mater. Sci. Eng. C*, 2020, **108**, 110444.
- 163 B. M. Dharmaraj, R. Subramani, G. Dhanaraj and K. Louis, *Compos. C: Open Access*, 2020, **3**, 10007–10019.
- 164 S. Mehnath and M. Jeyaraj, *Mater. Chem. Phys.*, 2023, **295**, 127061–127074.
- 165 J. Ji, C. Wang, Z. Xiong, Y. Pang and W. Sun, *Mater. Today Adv.*, 2022, **15**, 100259–100271.
- 166 S. Marchesi, F. Carniato, C. Bisio, L. Tei, M. Botta and L. Marchese, *Dalton Trans.*, 2018, **47**, 7896–7904.
- 167 S. Marchesi, D. Lalli, F. Carniato, C. Bisio, L. Tei, L. Marchese and M. Botta, *Dalton Trans.*, 2020, **49**, 6566–6571.
- 168 T. Zhou, L. Jia, Y. F. Luo, J. Xu, R. H. Chen, Z. J. Ge, T. L. Ma, H. Chen and T. F. Zhu, *J. Nanomed.*, 2016, **11**, 4765–4776.
- 169 G. Basina, G. Diamantopoulos, E. Devlin, V. Psycharis, S. M. Alhassan, M. Pissas, G. Hadjipanayis, A. Tomou, A. Bouras, C. Hadjipanayis and V. Tzitzios, *J. Mater. Chem. B*, 2022, **10**, 4935–4945.
- 170 M. V. Ramos-Garcés, J. González-Villegas, A. López-Cubero and J. L. Colón, *Acc. Mater. Res.*, 2021, **2**, 793–803.
- 171 A. Donnadio, G. Paul, M. Barbalinardo, V. Ambrogio, G. Pettinacci, T. Posati, C. Bisio, R. Vivani and M. Nocchetti, *Nanomaterials*, 2023, **13**, 742.
- 172 M. Pica, A. Donnadio, M. Casciola, *Coord. Chem. Rev.* 2018, **374**, 218–235.
- 173 M. L. González, M. Ortíz, C. Hernández, J. Cabán, A. Rodríguez, J. L. Colón and A. Báez, *J. Nanosci. Nanotechnol.*, 2016, **16**, 117–129.
- 174 J. González-Villegas, Y. Kan, V. I. Bakmutov, A. García-Vargas, M. Martínez, A. Clearfield and J. L. Colón, *Inorg. Chim. Acta*, 2017, **468**, 270–279.





Please do not adjust margins

- 175 H. Kalita, B.N. Prashanth Kumar, S. Konar, S. Tantubay, M. Kr. Mahto, M. Mandal and A. Pathak, *Mater. Sci. Eng. C*, 2016, **60**, 84–91.
- 176 H. Kalita, S. Rajput, B. N. P. Kumar, M. Mandal and A. Pathak, *RSC Adv.*, 2016, **6**, 21285.
- 177 S. Yu, X. Gao, H. Baigude, X. Hai, R. Zhang, X. Gao, B. Shen, Z. Li, Z. Tan and H. Su, *ACS Appl. Mater. Interfaces*, 2015, **7**, 5089–5096.
- 178 R. Hosseinzadeh and K. Khorsandi, *Scientific Reports*, 2019, **9**, 14899.
- 179 A. Donnadio, V. Ambrogio, D. Pietrella, M. Pica, G. Sorrentino and M. Casciola, *RSC Adv.*, 2016, **6**, 46249–46257.
- 180 I. García, C. Trobajo, Z. Amghouz and A. Adawy, *Materials*, 2021, **14**, 1481.
- 181 M. Pica, N. Messere, T. Felicetti, S. Sabatini, D. Pietrella and M. Nocchetti, *Materials*, 2021, **14**, 670.
- 182 H. Ueoka, O. Shimomura, M. Pica, A. Donnadio and R. Nomura, *Colloids Interface Sci. Commun.*, 2019, **28**, 29–33.
- 183 M. Bastianini, M. Sisani, A. Petracci, I. Di Guida, C. Faffa and F. Cardellini, *Mater. Adv.*, 2021, **2**, 1313–1319.
- 184 M. Camara-Torres, S. Duarte, R. Sinha, A. Egizabal, N. Alvarez, M. Bastianini, M. Sisani, P. Scopece, M. Scatto, A. Bonetto, A. Marcomini, A. Sanchez, A. Patelli, C. Mota and L. Moroni, *Bioact. Mater.*, 2021, **6**, 1073–1082.
- 185 H. Du, D. Zhang, F. Peng, K. W. K. Yeung and X. Liu, *Prog. Mater. Sci.*, 2024, **142**, 101220.
- 186 S. Kumari, V. Sharma, S. Soni, A. Sharma, A. Thakur, S. Kumar, K. Dhama, A. K. Sharma and S. K. Bhatia, *Environ. Res.*, 2023, **238**, 117171.
- 187 Y. Bian, X. Cai, Z. Lv, Y. Xu, H. Wang, C. Tan, R. Liang and X. Weng, *Adv. Sci.*, 2023, **10**, 2301806.
- 188 S. Karimi, H. Rasuli and R. Mohammadi, *Int. J. Biol. Macromol.*, 2023, **234**, 123538.
- 189 V. R. Leopoldo Constantino, M. P. Figueiredo, V. R. Magri, D. Eulalio, V. R. Rodrigues Cunha, A. C. Santos Alcantara and G. F. Perotti, *Pharmaceutics*, 2023, **15**, 413.
- 190 C. Nomicisio, M. Ruggeri, E. Bianchi, B. Viganì, C. Valentino, C. Aguzzi, C. Viseras, S. Rossi and G. Sandri, *Pharmaceutics*, 2023, **15**, 1368.
- 191 Q. Li, X. Wu, S. Mu, C. He, X. Ren, X. Luo, M. Adeli, X. Han, L. Ma and C. Cheng, *Adv. Sci.*, 2023, **10**, 2207759.
- 192 J-H. Yang, J-H. Lee, H-J. Ryu, A. A. Elzatahry, Z. A. Allothman and J-H. Choy, *Appl. Clay Sci.*, 2016, **130**, 20–32.
- 193 G. Choi, S. Eom, A. Vinu and J-H. Choy, *Chem. Rec.*, 2018, **18**, 1033–1053.
- 194 S. S. Shafiei, M. Shavandi, G. Ahangari and F. Shokrolahi, *Appl. Clay Sci.*, 2016, **127**, 52–63.
- 195 F. Perreault, A. Fonseca de Faria, S. Nejati and M. Elimelech, *ACS Nano*, 2015, **9**(7), 7226–7236.
- 196 G. Reina, J-M. Gonzalez-Dominguez, A. Criado, E. Vazquez, A. Bianco and M. Prato, Maurizio, *Chem. Soc. Rev.*, 2017, **46**(15), 4400–4416.
- 197 P. Das, S. Manna, A. K. Behera, M. Shee, P. Basak, A. K. Sharma, *Environ. Res.*, 2022, **212**, 113534–123546.
- 198 R. Mukhopadhyay, D. Bhaduri, B. Sarkar, R. Rusmin, D. Hou, R. Khanam, S. Sarkar, J. Kumar Biswas, M. Vithanage, A. Bhatnagar and Y. S. Ok, *J. Hazard. Mater.*, 2020, **383**, 121125.
- 199 X. Fu, J. Lin, Z. Liang, R. Yao, W. Wu, Z. Fang, W. Zou, Z. Wu, H. Ning and J. Peng, *Surf. Interf.*, 2023, **37**, 102747.
- 200 S. Gungordu Er, M. Edirisinghe and T. A. Tabish, *Adv. Healthcare Mater.* 2023, **12**, 2201523.
- 201 X. You, Q. Zhang, J. Yang and S. Dong, *Compos. - A: Appl. Sci.*, 2023, **167**, 107420.
- 202 S. Ren, M. Cui, C. Liu and L. Wang, *Corros. Sci.*, 2023, **212**, 110939.
- 203 M. Rahaman, L. Nayak, I. A. Hussein, N. C. Das (Eds.). Polymer Nanocomposites Containing Graphene: Preparation, Properties, and Applications. Woodhead Publishing, 202.
- 204 C. Cheng, W. Song, Q. Zhao and H. Zhang, *Nanotec. Rev.*, 2020, **9**, 323–344.
- 205 H.W. Huang, X.X. Sheng, Y.Q. Tian, L. Zhang, Y. Chen and X.Y. Zhang, *Ind. Eng. Chem. Res.*, 2020, **59** (35), 15424–15446.
- 206 H. Huang, M. Li, Y. Tian, Y. Xie, X. Sheng, X. Jiang and X. Zhang, *Prog. Org. Coat.* 2020, **138**, 105390.
- 207 T.C. Huang, G.H. Lai, C.E. Li, M.W. Tsai, P.Y. Wang, Y. H. Chung and M. H. Lin, *RSC Adv.*, 2017, **7** (36), 22540–22540.
- 208 S.L. Li, C.X. Zhao, H.L. Gou, Y.T. Li, X.J. He and L. Zhao, *Int. J. Electrochem. Sci.*, 2018, **13** (3), 2661–2675.
- 209 C.X. Zhao, P. Li, D. He, Y.T. Li, F. Lei, and H.J. Sue, *RSC Adv.*, 2016, **6**, 73485–73495.
- 210 Y.F. Xiao, J.Y. Xu, S.W. Huang and H.M. Deng, *Int. J. Polym. Sci.* 2017, 6034741.
- 211 K.Q. Li, H.M. Lei, X.R. Zeng, H.Q. Li, X.J. Lai and S.Y. Chai, *RSC Adv.*, 2017, **7**, 49290–49298.
- 212 L.F. Xu, C.H. Lei, R.J. Xu, X.Q. Zhang and F. Zhang, *Polym. Degrad. Stabil.*, 2016, **133**, 378–388.
- 213 L.F. Xu, C.H. Lei, R.J. Xu, X.Q. Zhang and F. Zhang, *RSC Adv.*, 2016, **6**, 77545–77552.
- 214 E.N. Kalali, S. De Juan, X. Wang, S. Nie, R. Wang, D-Y. Wang, *J. Therm. Anal.*, 2015, **121**, 619–626.
- 215 D.D. Yang, Y. Hu, H.T. Li, L. Song, H.P. Xu and B. Li, *J. Therm. Anal*, 2015, **119**, 619–624.
- 216 D. Wang, H.Y. Peng, B. Yu, K.Q. Zhou, H.F. Pan, L.P. Zhang, M. Li, M. Liu, A.L. Tian and S.H. Fu, *Chem. Eng. J.*, 2020, **389**, 124449.
- 217 B. Ghanbarzadeh, S.A. Oleyaei and H. Almasi, *Crit. Rev. Food Sci. Nutr.* 2015, **55**, 1699–1723.
- 218 D. Han, Y. Luo, Q. Ju, X. Xiao, M. Xiao, N. Xiao, S. Chen, X. Peng, S. Wang and Y. Meng, *Polymers* 2018, **10**, 1082.
- 219 H. Oosthuizen, L. Jones, S. Naseem, F. J. W. J. Labuschagne and A. Leuteritz, *J. Polym. Sci.*, 2023, **61**, 1749–1777.
- 220 S. Kumari, S. Soni, Aj. Sharma, S. Kumar, V. Sharma, V. S. Jaswal, S. K. Bhatia and A. K. Sharma, *Appl. Clay Sci.*, 2024, **247**, 107216.
- 221 Y. Guo, F. Leroux, W. Tian, D. Li, P. Tang and Y. Feng, *Appl. Clay Sci.*, 2021, **211**, 106198.
- 222 A.A. Marek, V. Verney, G. Totaro, L. Sisti, A. Celli, N. Bozzi Cionci, D. Di Gioia, L. Massacrier, and F. Leroux, *Appl. Clay Sci.*, 2020, **188**, 105502.



Please do not adjust margins

- 223 S. Coiai, F. Cicogna, S. Pinna, R. Spiniello, M. Onor, W. Oberhauser, M-B. Coltelli and E. Passaglia, *Appl. Clay Sci.*, 2021, **214**, 106276.
- 224 Q. Zhang, Y. Guo, F. Leroux, P. Tang, D. Li, L. Wang, and Y. Feng, *New J. Chem.*, 2020, **44** (24), 10119-10126.
- 225 J. Zhang, Q. Ke, J. Bai and M. Yang, *Polym. Degrad. Stab.*, 2023, **218**, 110550.
- 226 L. Han, J. Geng, Z. Wang and J. Hua, *Polym. Adv. Technol.*, 2022, **33**, 3619-3627.
- 227 Y. Feng, Y. Jiang, Q. Huang, S. Chen, F. Zhang, P. Tang and D. Li, *Ind. Eng. Chem. Res.* 2014, **53** (6), 2287-2292.
- 228 Q. Zhang, Y. Guo, A.A. Marek, V. Verney, F. Leroux, P. Tang, D. Li and Y. Feng, *Inorg. Chem. Front.*, 2019, **6**, 2539-2549.
- 229 Q. Zhang, Q. Gu, F. Leroux, P. Tang, D. Li and Y. Feng, *Beilstein J. Nanotechnol.* 2018, **9**, 2980-2988.
- 230 N. K. Kumbhar, M. D. Joshi, V. Kumar and S. S. Hosmani, *Adv. Eng. Mater.*, 2023, **25**, 2201680.
- 231 A. Chaouiki, M. Chafiq, T. Suhartono and Y. G. Ko, *Chem. Eng. J.*, 2023, **470**, 144355.
- 232 F. G. Nunes F., E. C. Silva F., J.A: Osajima, A.P. de Melo Alves, M.G. Fonseca, *Appl. Clay Sci.*, 2023, **239**, 106952.
- 233 Z. Chen, G.-F. Han, A. Mahmood, J. Hou, W. Wei, H. Kyong Shon, G. Wang, T. D. Waite, J.-B. Baek and B.-J. Ni, *Prog. Mater. Sci.*, 2024, **145**, 101299,
- 234 D. Evis, M.M. Ba-Abbad, A. Benamor, M. H. El-naas, *Appl. Clay Sci.*, 2022, **229**, 106686
- 235 C. Zhu, J. Jiang, Y. Jia, Z. P. Xu and L. Zhang, *Acc. Mater. Res.*, 2023, **4**, 758-771.
- 236 H. Desai, K. A, G. S. K. Reddy, *Microp. Mesop. Mater.*, 2023, **352**, 112488.

View Article Online  
DOI: 10.1039/D4DT00757C

